Solar Energetic Particles and their Measurements with Space Borne Instruments

Master's thesis
University of Turku
Department of Physics and Astronomy
Astronomy
July 2021
BSc Lary Adam Salifu
Examiners:
Prof. Rami Vainio
Dr. Silja Pohjolainen

According to the University of Turku quality control this text has been checked with Turnitin Originality Check.

UNIVERSITY OF TURKU
Department of Physics and Astronomy
LARY ADAM SALIFU: Solar Energetic Particles and their Measurements with Space Borne Instruments
Master's thesis, 50 pages
Astronomy
July 2021

The study of our Sun and its various modes of activity is an important area of research in the field of space physics and heliophysics. These active phenomena such as solar flares and Coronal Mass Ejections are associated with energetic particles (protons, electrons, ions, etc.) which are released into our solar system and possess high speed. Some of these energetic particles are likely to reach Earth. In this work, I looked into the various types of solar particle events and their characteristics as well as how these energetic particle properties are measured using space borne instruments. Different instruments using different measurement techniques were also studied, which gives us information about the kind of energetic particles that are measured or detected by these different instruments. A design of a particle telescope, which employs the use of multiple detectors was studied in this work. The telescope had three Si-detectors, a foil material (Kapton polyimide film) and a caesium iodide (CsI) detector. The detector thicknesses were optimised in order to achieve a desired result. Thus in total the design had four detectors and an entrance foil. The thicknesses of the foil material and CsI detector were as well converted into their respective silicon range equivalence in order to optimise the layer thicknesses in the design. Particles are measured at different angles of incidence but for the purpose of this work, I looked at particles penetrating the detectors at 0º and 25º as the limiting values. The results show that the minimum energies a particle needs to penetrate the foil material at 0º and 25º are 4.97 MeV and 5.27 MeV respectively. The effective threshold energy of protons detected in the first detector (D1) is between these values. Furthermore the results give us the information that as the angle of incidence is increasing, the energy also increases steadily. The energy channel resolution for protons stopping in D1, D2 and D3 were 0.386, 0.355 and 0.374 respectively which was close to the desired value (0.4) set as a target of the design.

Key words: Solar Energetic Particles, Coronal Mass Ejections, Solid State Detectors, Scintillators, Particle telescopes, Cosmic rays, Radiation belts.

Contents

1. Introduction

Our Sun is very vital in the field of astronomy and space physics due to its several characteristics and properties. In the solar system, the sun is viewed as a significant emitter of energetic particles. The particles are known to range from suprathermal (few keV) to relativistic energies and are observed in-situ as solar energetic particle (SEP) events by radiation detectors on-board satellites. Active phenomena of the Sun for example solar flares and coronal mass ejections (CMEs) stands out as driving source of SEPs [Rodriguez-Pacheco et al., 2020].

As a significant area of research in space physics and heliophysics, the Sun undergoes active phenomena making its surface very busy with many events occurring on its surface. The Sun also generates magnetic fields as a result of electric currents carried by the charged particles of its interior and atmosphere. The gases in the interior and the atmosphere of the Sun are in constant motion and as a result, they tangle, stretch and twist the magnetic fields generated. Solar activity therefore, can be defined as the various events (solar flares, CMEs, high speed solar wind, etc.) that takes place on the exterior space of the Sun and its effects it surrounding space.

Solar flares are a sudden release of energy from the Sun. This phenomenon occurs when the energy deposited within the magnetic field close to sunspots are released. A magnetic re-alignment also plays a major role during release of energy. The energy associated with these flares is high (10^{25} joules). These flares occur low in the corona, heat up plasma to very high temperatures (tens of millions of degrees) and accelerate particles (electrons, protons and heavier ions) close to the speed of light. Also solar flares can emit radiation across the entire electromagnetic (EM) spectrum from radio waves to x-rays and gamma-rays. These radiations are released into space. Solar flares also are sometimes accompanied by CMEs, which can accelerate to high velocities into space when the Sun's magnetic fields reorganize suddenly [Wang, 2009].

There are several mechanisms in charged particle acceleration to higher energies that occur in our universe. These mechanisms include solar flares, acceleration by reconnecting current sheets, turbulence and shocks. Solar flares, as mentioned earlier, are often associated with CMEs. The mechanism responsible for accelerating powerful explosions to higher energies is the solar flare mechanism. This acceleration is as a result of fast magnetic reconnection, sudden

reconfiguration of the magnetic topology and also the associated magnetic energy released. These characteristics are regarded as the main driving force/engine for which powerful explosions are accelerated to such higher energies. The magnetic energies released during particle acceleration is converted kinetic energy and mechanism still remain uncertain [Miller, et al., 1997, Zharkova, et al., 2011]. Particle acceleration within our solar system is also attributed to solar eruptions and their associated shock waves. Termination shock (TS) produced by the fast reconnection outflows striking on dense, closed loops in a helmet type geometry is a possible candidate which is usually raised in the standard picture of solar eruptions. The significance of TS in solar particle acceleration remains quite controversial mainly due to the inability to directly detect particle acceleration in such shocks [Gary et al., 2015, Forbes, 1986].

The observational evidence of the TS has been cited to be certain radio sources depicting spectroscopic features that are similar to the solar type II radio burst (radio emission associated with propagating shocks in the outer corona). These sources have a small drift in their emission frequency as a function of time compared to the solar type II radio burst, which implies an almost standing shock wave. [Aurass, et al., 2002].

The acceleration site is very often aligned to the open magnetic field lines and the effect is a high probability of having energized particles entering into the interplanetary medium. These energetic particles are examined by spacecraft away from their acceleration sites as velocity-dispersed bursts. Faster particles arrive more quickly as expected when particles of all energies are accelerated at the Sun simultaneously and then travel at equal distance along the IMF to reach the spacecraft. These bursts of energetic particles are referred to as SEP events.

Available records shows that SEP activities has earlier been observed to be higher as they increase in the intensity in ground level ion chambers on February 28 and March, 1942[Forbush, 1946] and each accompanying a remarkably bigger solar flare. The rise are influenced by energetic protons (~ 1 GeV) pushing into the neutral atmosphere of the Earth. Later solar radio wave observations suggested that two accelerators were involved in “solar flares and coronal/interplanetary shock waves. Fast-drifting type III radio bursts are the hallmark of the particle acceleration process in solar flares, while slow-drifting type II bursts show the acceleration by coronal shock waves. [Wang, 2009]

Following the discovery of CMEs in the 1970s, [Wang, 2009] is reported to have found a connection between large solar proton events and fast CMEs, and in some case, even large SEP that didn't have flares. These findings reveals that besides the already known solar flares, shock waves occassioned by fast CMEs are another accelerator option for SEP events and they are responsible for the occurrence of gradual SEP events [Hu, 2017].

Indeed, the need to establish ways through which particles are being accelerated from the sun into the interplanetary space has become very important owing to the diverse views among scholars concerning this phenomenon or event. Over the years, it has been widely accepted that CME-driven shocks are more or less the only or main agent for particle acceleration in large SEP events [Reames, 1999]. However, CME driven shocks are not the only particle accelerators but also shock drift are also particle accelerators in SEPs. In fact, further reading has pointed out that "shock drift acceleration", "shock surfing acceleration" and "diffuse shock acceleration" are important particle accelerators in solar particle events or solar energetic particles [Rodriguez-Pacheco et al., 2020]. To explain further, it can be argued that the acceleration are as a result of shock properties and seed population. [Rodriguez-Pacheco et al., 2020]. And CMEs are the main particle accelerators for gradual SEP events. [Rodriguez-Pacheco et al., 2020].

Solar flares are associated with magnetic reconnection making them responsible for the existence of "impulsive SEP events which are enriched in electrons, helium (He) and heavier ions such as Ne-Fe" [Mason, 2007] "while large scale shock waves and their related processes driven by fast CMEs are associated with gradual SEP events" [Reames, 1999]. These two distinct energetic particle accelerators are extremely efficient and the eventual outcome is such "that charged particles are energized up to GeV energies within a" short period of time [Rice et al., 2003].

2. Energetic Particle Populations in Space

The main topic of this thesis project is energetic particles and their measurement in space. Energetic particles are particles that possess an energy exceeding the thermal energy of plasma. They are ionized particles and their energies are from a few kiloelectronvolts (keV) up to several gigaelectronvolts (GeV) (ratio of a million) when accelerated in our own heliosphere. There are several different populations of heliospheric particles, as depicted in Fig. 2.1. Other energetic particles such as cosmic rays have energies up to 10^{20}eV. Galactic cosmic rays are accelerated in our own galaxy, e.g., in supernova remnants and pulsar magnetospheres. Extra-galactic cosmic rays are accelerated in sources outside the Milky Way, e.g., in extragalactic jets of active galactic nuclei, harboring relativistic shock waves. The highest energies of galactic cosmic rays are probably not extending to 10^{20} eV, but are rather somewhere in the range from 10^{15} eV to 10^{18} eV. Energetic particles are composed of mainly protons, electrons and Helium nuclei (alpha particles). In some cases there are small contributions of heavy ions extending to iron and beyond.

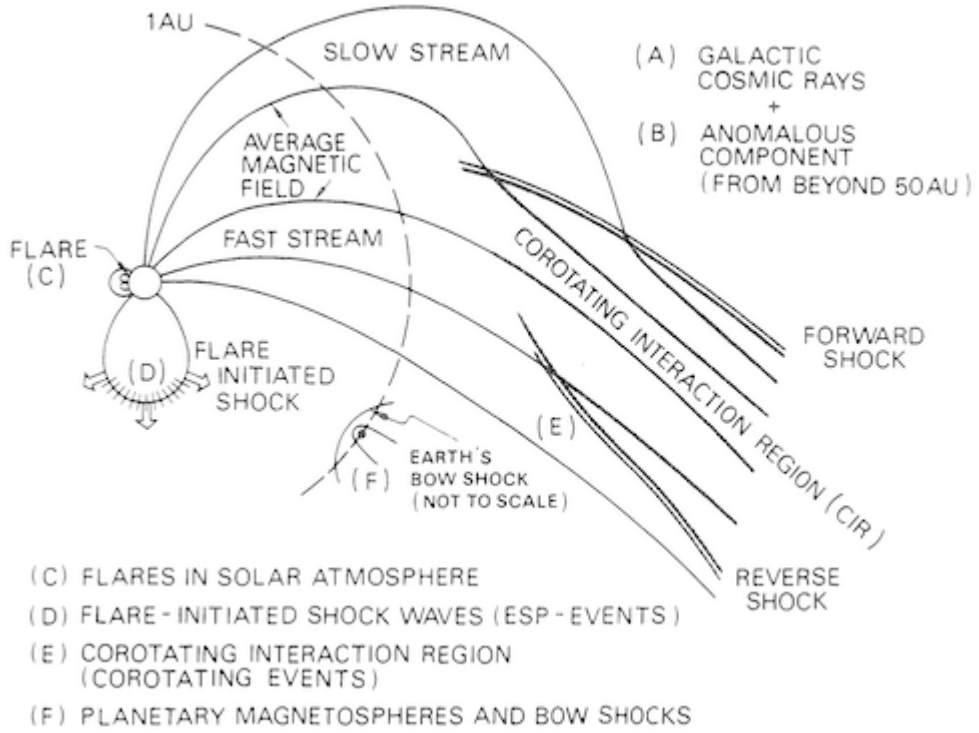

Fig.2.1 schematic representation of the various energetic particles components and their sources. Image credit: Kunow et al. [1991]

Based on the different environments existing within the inner solar system, there are many kinds of particle populations in it that vary by

- temporal characteristics
- spectra (energy)
- composition (particle distribution)
- charge state
- anisotropies

Sources of energetic particles are

- Sun and solar activity
- Interplanetary space (solar wind acceleration)
- Planetary magnetospheres
- Galactic and extra-galactic sources (outside of the solar system)

2.1 Galactic Cosmic Rays

The sources of galactic cosmic rays are located inside the Milky Way. These particles are usually assumed to be produced in shock waves that develop in supernova explosions. These supernova explosions are energetic events that occur when stars near the end of their life. They explode and shed a significant amount of their material. In the process, shock waves are generated that propagate very fast with lots of energy. They can as well accelerate ionized particles. Unlike solar energetic particles, galactic cosmic rays measured at Earth are anti-correlated to the sunspot number. At sunspot maximum, galactic cosmic rays are on the minimum and vice-versa (see fig. 2.2). This is as a result of galactic cosmic rays being modulated because of the magnetic flux shed by the Sun in the form of CMEs, but solar wind turbulence and stream interaction regions also have a role to play.

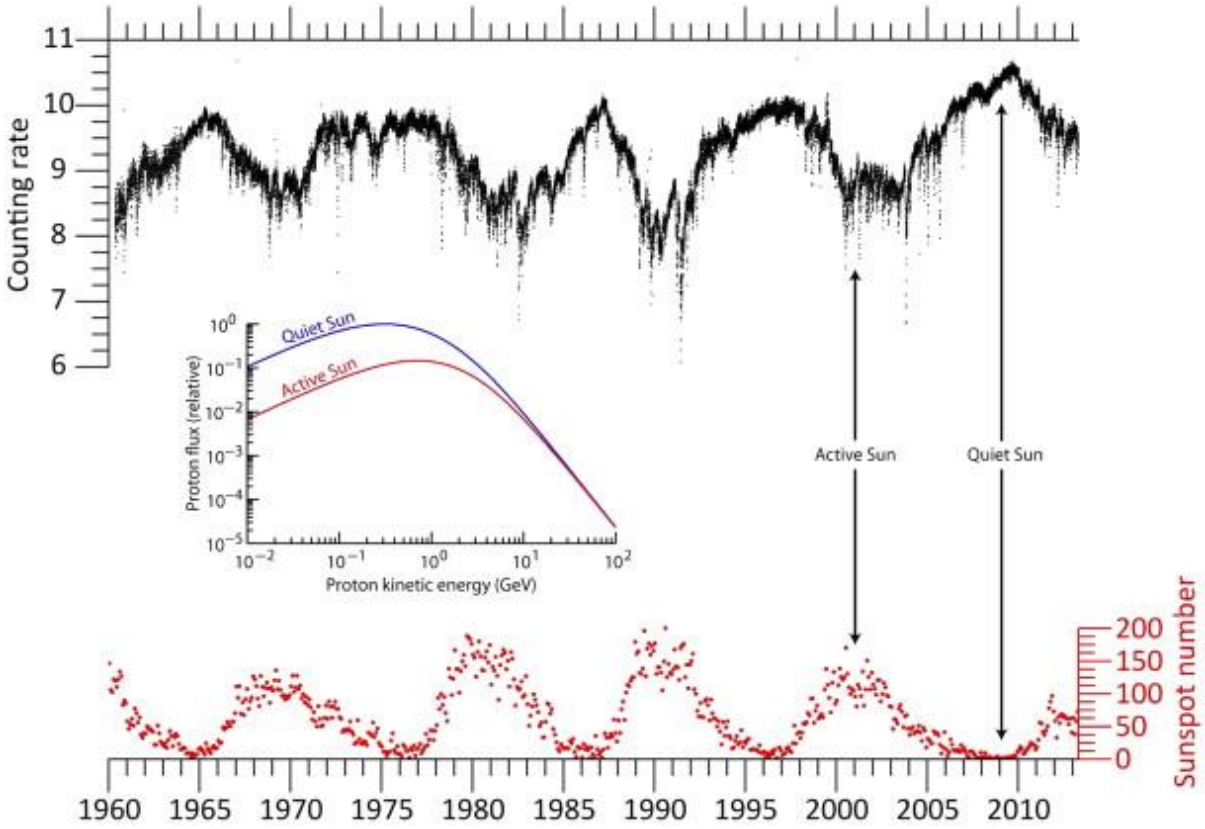

Fig.2.2 Neutron counting rates variation (with units of 10^5 counts per hour) measured at McMurdo Station in Antarctica as a function of time, cosmic ray spectrum and time series of sunspot number. Image credit: Prettyman, [2014].

Cosmic rays also generate a nuclear cascade that produces neutrons which reach the ground level and can be detected by neutron monitors. This happens when the cosmic rays penetrate the atmosphere. In figure 2.2 the monthly sunspot counts are compared to cosmic-ray induced neutron monitor counting rates. In the process of low solar activity (low sunspot counts), low-energy galactic cosmic rays permeate the heliosphere, and consequently generate a somewhat high atmospheric neutron production rates by cosmic rays. However, in the course of high solar activity (high sunspot counts), the low-energy galactic cosmic rays are cut off, bringing about a lower neutron counting rates. The difference in neutron counting rates is about 20% over the solar cycle. Also theoretical galactic proton energy spectra within the heliosphere, representing the quiet and active solar years, is shown (inset) [Prettyman, 2014]. Cosmic rays and their relation to other space environment parameters are presented in Fig. 2.3.

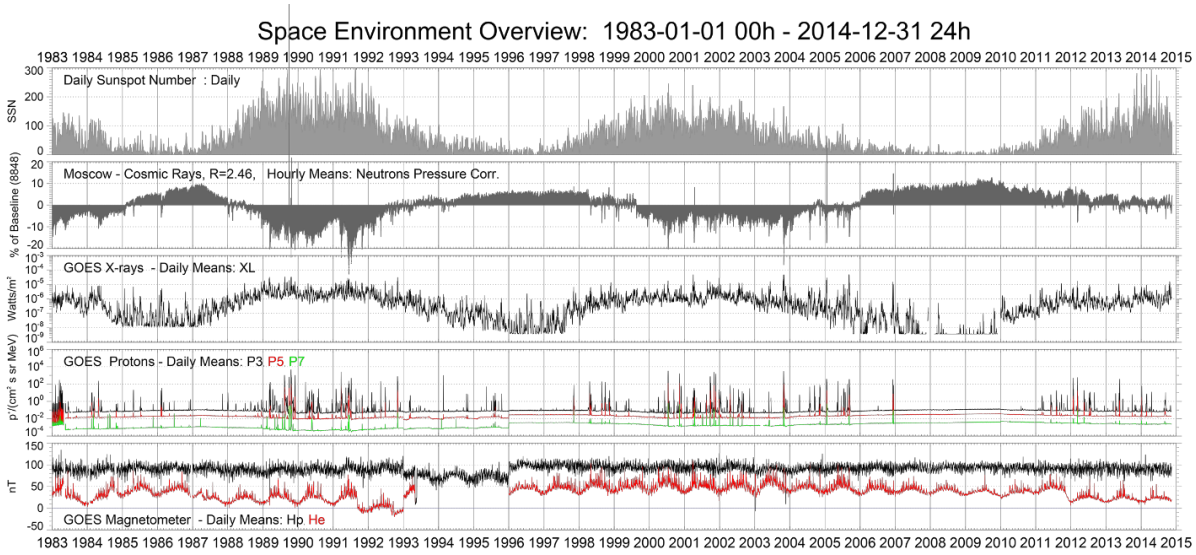

Fig. 2.3. An overview of three solar cycles showing the relationship between the sunspot cycle, galactic cosmic rays and the state of our near space environment. Image credit: Hu [2017].

Anomalous cosmic rays are energetic particles created far out in the solar system at distances beyond 50 AU. Their existence is quite interesting and so is the process of their creation in the heliosphere when the solar wind and low-energy neutral atoms interact. Anomalous cosmic rays are accelerated as charged particles in the outer heliosphere, but the mechanism is still not fully understood. One candidate is the solar wind termination shock. The origin of these ions that are accelerated in the shock is the ionisation of interstellar neutrals and a following pick-up process that generates so-called pick-up ions at suprathermal energies. These are singly charged and more mobile than the multiply ionised thermal solar-wind particles. They get more easily accelerated at the termination shock than thermal ions and can be observed as an additional cosmic-ray population with low charge states and energy spectra peaking below the peak energy of the galactic cosmic ray energy spectrum.

2.2 Solar energetic particles (SEPs)

SEP events mostly occur when particles (e.g., protons) are emitted by our Sun. These particles are accelerated either close to the Sun during a flare or in the interplanetary space by CME-driven shocks. Research suggests that not more than 1% of CMEs produce strong SEP events. Wide and fast CMEs are much more likely to generate SEP events than CMEs on average. Typically these events also include helium ions and high atomic number energetic (HZE) ions causing many kinds of radiation effects on spacecraft. [Hu, 2017]

SEPs are able to penetrate the Earth's magnetic field causing ionization within the ionosphere. This phenomenon can be liken to that of auroral events but in this regard protons are the energetic particles involved. Astronauts onboard a spacecraft as well as the spacecraft itselt suffer a significant radiation hazard from energetic particles (ions). [Hu, 2017]

Solar protons are mostly associated with insufficient energies and as a result they are not able to penetrate through the Earth's magnetic field. Strong flares however provide protons with sufficient energies in order for the protons to get to the Earth's magnetosphere and ionosphere encircling the Earth's poles. These energetic particles (protons) exit the surface of the Sun and due to their charged nature, they stick to the Sun's powerful magnetic fields. Furthermore, upon entering the Earth's region (magnetosphere) which have fields much powerful than those existing in the interplanetary space, these particles continue to align themselves and stick to the Earth's magnetic field leading them into the Earth's polar regions where the Earth's majority field lines (magnetic) connect to the solar wind.

There is a collusion of energetic protons that are channelled into the polar regions with atmospheric elements and in the process of ionization their energies are released. Most of these energies are turn-off at the lower base region of the ionosphere (50 – 80 km in altitude). The lower base region of the ionosphere is vital to ionospheric radio communications and majority of the intake of radio signal energy takes place in this region of the ionosphere.

A high intensity of solar protons flashes up with the potential of generating a high energetic protons (in surplus of 500 MeV) with an impact of escalating the neutron count rates at lower levels through a subordinate radiation effects known as the ground level enhancement (GLE). An important proton radiation exposure is mostly encountered by astronauts outside of the Earth's magnetosphere protective shield. This could occur e.g., when astronauts are at the orbit, surface or in transit to the Moon. This effect is reduced when astronauts are at the lower orbit of the Earth and also, restricted to many protected regions of their spacecraft. Again, when the spacecraft gets closer to the polar regions, there is a greater exposure to solar energetic protons radiation due to proton radiation levels found in low Earth orbit that influences orbital inclination. [https://en.wikipedia.org/wiki?curid=38180478, accessed 1.7.2021]

SEPs are also an interesting area of study as they provide us with a typical solar material. Notwithstanding the nuclear fusion which takes place within the core, the larger part of the solar material is an indication of the material that formed our solar system. Examining the isotopic configuration/structure of the SEPs, researchers are able to obliquely compute the material that have formed our solar system [see Reames, 1999, for review]. SEPs provide samples of solar material that is used to determine the isotopic composition of the Sun. In gradual SEP events, accelerated particles are either associated with solar wind or coronal material which are boosted by large shocks powered/propelled by CMEs. Also in gradual SEP events, elemental abundances are mostly changing from one event to the other and they correspond with the ionic charge to mass ratio, Q/M [Leske et al., 2001]. SEP abundances discloses the coronal elemental configuration after the fractionation is corrected or averaging over multiple events [Reames, 1995, Leske et al., 2001]. In this regard, the coronal isotopic composition can also be obtained from SEPs [Leske et al., 2001].

2.2.1 Classes of Solar Energetic Particles

Generally, there are two accepted types of SEP events that occur within our solar system namely the impulsive SEP events which are directly related to the solar flares and the gradual SEP events which are also being caused by CMEs [Desai and Giacalone, 2016]. In these classes of events, energies are released fast and slowly over a time period, respectively. Table 2.1 below gives the various characteristics of the two classes of SEP's events.

Table 2.1. The two classes of SEP events [from Reames, 1995b; Kallenrode, 2003]

Characteristic	**Large SEP events (Gradual SEP events)**	**Electron/3He-rich SEP events (Impulsive SEP events)**
Dominant particle species	>~ 10 MeV protons	~ 1 - 100 keV electrons
Electron/proton ratio	small	large
$^3He/^4He$	'normal' coronal - 0.0004	~ 1
Heavy nuclei	'normal' coronal	enhanced abundances of Fe, Mg, Si, S
Fe/O	~0.1	~1
Q_{Fe}	~ 14	~20 for Fe , ~ 14 for Si
Duration	Days	hours
Longitude cone	>~ 100°	<~ 30°
Event rate (at solar max.)	~ 10/year	>~ 1000/year
Association Flares	large flares (but sometimes missing)	mostly small flares but often no flares
Soft X-ray bursts	gradual (~ hours)	impulsive (< 10s min)
CMEs	fast CMEs	—
Radio bursts	type II	type III

Figure 2.4 depicts sketches of the two SEP acceleration scenarios. "SEP events are generally classified as 'gradual' and 'impulsive' because the associated soft X-ray burst (when present) is of long duration and of short duration respectively [see Reames, 1999, for review]. However the terms 'gradual' and 'impulsive' do not efficiently resolve the particle acceleration mechanisms". [Wang, 2009]

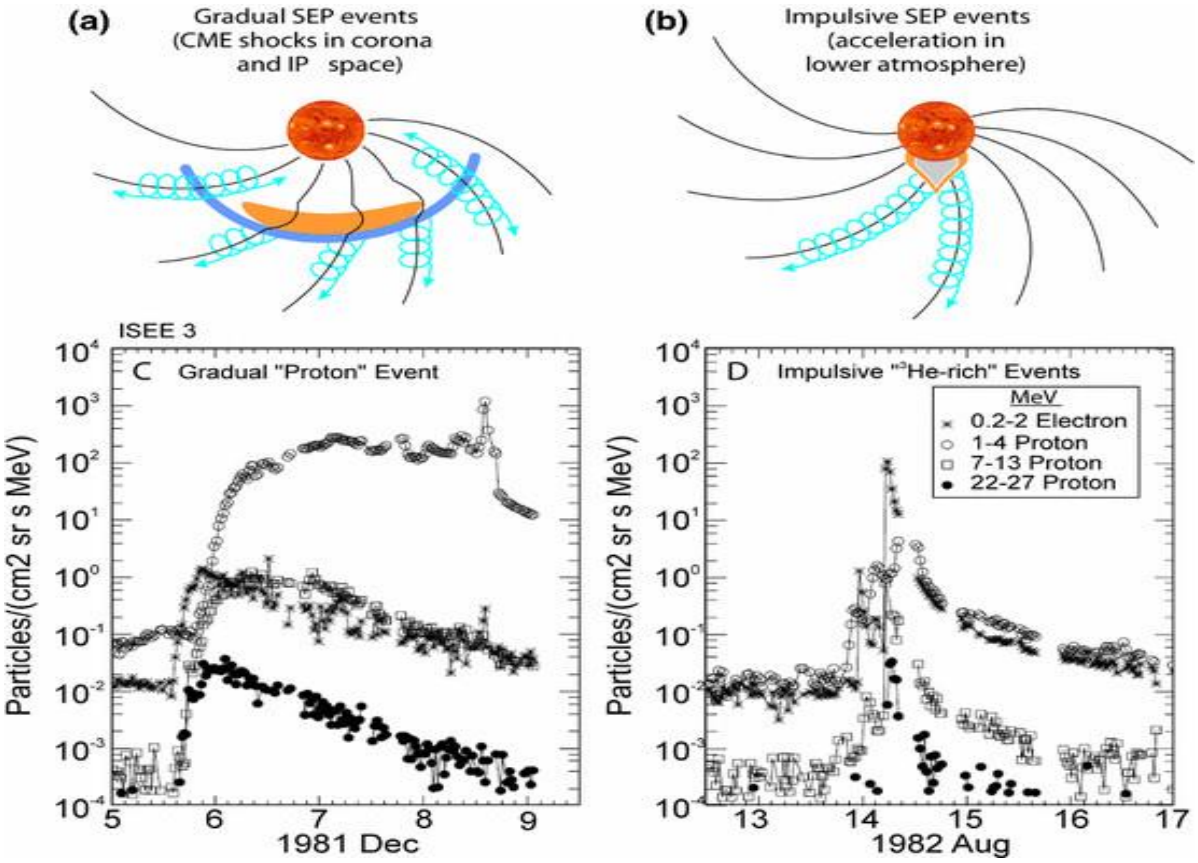

Fig. 2.4 The classification of SEP events where (a) and (b) are gradual SEP event produced by large scale CME-powered shock and impulsive SEP event produced by solar flare respectively. (c) and (d) are large gradual events and small impulsive events respectively. Image credit: Reames [1999]

2.2.1.1 Gradual SEP Events

This energetic particle class of event is one that occurs over a prolonged period of time (days) with protons being the main dominant species (i.e., has small electron-to-proton ratios). The energies in this class of event are in the range of GeV corresponding to large particle intensities. This class of events has also characteristics of normal coronal abundances (e.g., ^{3}He / ^{4}He ~0.0004) and charge states corresponding to the typical quiet coronal temperatures of ~1 – 2 x10^6 K. This class of events has an occurrence rate of 10/year at solar maximum extending to 100º-180º in solar longitude and is strongly associated with solar flares, fast CMEs and type II radio bursts and most importantly this event class is accelerated by CME-driven shocks [Wang, 2009].

2.2.2.2 Impulsive SEP Events

This class of events is dominated by ~1 – 100 keV electrons (high electron to proton ratios). Also they are characterized by MeV/nucleon ion emissions with small intensities of particles, enhanced. 3He / ^{4}He ratios up to 10^4 times that of the coronal values. Impulsive SEP events last for a short period of time (hours) due to their characteristics and also span 30° in longitude. They are associated with type III radio bursts and small flares, but flares could also be missing. [Wang, 2009]

At solar maximum, these events have occurrence rate of >1000/year across the entire surface of the Sun, representing the most common impulsive solar particle acceleration phenomenon. They have an average ionization state of ~20 for Fe and ~14 for Si interpreted as being either heating to temperatures of ~10^7 K or stripping of the ions by intense electron beams in impulsive flares. [Wang, 2009]

2.3 Trapped Particles

Our Sun's activity is not the only source of energetic particles that has been discussed in this work. The planets and their interactions with the interplanetary medium provide another rich source of energetic particles. Generally, energetic particles are found in three distinct regions namely the planetary bow shocks, inner magnetospheres and the dynamic regions of the outer magnetospheres [Reames, 1999]. For example particles are stably trapped in well-defined regions in Earth's magnetic field as a result of the interaction of the galactic cosmic radiation as well as the solar cosmic radiation with the Earth's magnetic field and the atmosphere.

Around our Earth is a zone occupied by energetic charged particles emanating mostly from solar wind. These energetic particles are mainly electrons and protons. [Reames, 1999]. Neutrons that are products as a result of nuclear interactions of the galactic cosmic rays with nuclei of the atmosphere are projected upward into the magnetic field region. These projected particles (neutrons) within the magnetic field region decay to produce stably trapped protons and electrons [Reames, 1999]. The trapped particles (protons) have a spectrum which inversely decreases with energy (1 MeV to 1 GeV). The spectrum is somewhat flattened at very low energies as a result of increase in energy losses. [Reames, 1999]

During large SEP events, it is possible to form temporary radiation belts when the associated CME and shock strikes the Earth [Reames, 1999]. Within the magnetosphere, a large disturbance permits sudden trapping of SEP ions as well as electrons filled in the outer magnetosphere [Reames, 1999]. The new radiation belts are capable of lasting for periods of months and observations within these belts are confined to just protons and electrons. However, we can predict SEP-like abundances are present within these belts.

3. Detection methods for energetic particles in space

3.1 Detector Types

3.1.1 Semiconductor/solid state detectors

Semiconductor materials have been one of the successes in the area of energetic particle detection. This is because particle detectors made from semiconductor materials depend on several characteristic properties that seem unavailable in other detector types. The benefits of such a detector material are a combination of extremely precise energy measurement of energetic particles and a possibility to determine also the position of the particle hitting the detector. These detectors also come with high-speed readout electronic systems, direct availability of signals in electronic form, as well as the possibility of integrating the detector and readout electronics on a common substrate [Rizzi et al., 2010].

The semiconductor material usually used in the design of the detectors is silicon (Si) or germanium (Ge) due to their excellence in energy resolution. Silicon on the other hand is characterized by low stopping power for photons with high energy while germanium only operates at cryogenic temperature due to its small band gap nature [Rizzi et al., 2010]. In other to achieve high efficiency detectors, compound semiconductors (eg., GaAs, CdTe, etc.) are studied in that regard. [Rizzi et al., 2010]

Semiconductor materials are selected based on the specific application as well as the energy range of interest in order to achieve the desired result. In the design of detectors, close attention is given to semiconductor growth, device structure as well as technological processes. This is because both detectors and detection methods are currently fields of development and investigations. Some characteristic parameters are also introduced in designing the detectors which gives us the detector performance needed [Rizzi et al., 2010].

3.1.1.1 Properties of semiconductor

Elemental semiconductors are materials found on the periodic table mostly as group IV elements (i.e., they have four electrons in their outermost shell). Electron energy levels in all elements are organized in bands (valence band, band-gap and conduction band). The lower band (valence band) has electrons which are bound to lattice sites within the crystal while the

upper band (conduction band) is characterized by free electrons which contribute to the conductivity of the material [Rizzi et al., 2010].

The valence band and conduction band are separated by a band-gap. The band-gap is vital as its dimensions define the class of a material (element) as conductor, semiconductor or insulator. In the absence of an external applied field which causes lattice vibration providing electrons with enough energy, a semiconductor will exhibit a valence band filled with electrons while its conduction band remains vacant. For electrons bound in the valence band to acquire enough energy and move into the conduction band, an energy high enough than that of the band-gap is applied to the electrons. The vacancy created by the transferred electrons into the conduction band is termed as hole. The mean displacement of movable charge carriers due to random motion is zero but owing to the application of an electrical field, both electrons inside the conduction band and holes inside the valence band can freely move and they contribute to the conductivity of the material [Rizzi et al., 2010].

Introducing a small amount of different elements with different atomic structure into a semiconductor is another method of obtaining free electrons or free holes as majority charge carriers. These elements are called dopants or impurities. To obtain a free electron the semiconductor is doped with a pentavalent element (i.e., element with five electrons in its outermost shell) while for a free hole it is doped with a trivalent element (i.e., element with three electrons in its outermost shell). In this way the electrical properties of the pure semiconductor material can be modified and controlled [Rizzi et al., 2010]. When the semiconductor has a free electron after doping, the majority charge carrier is the electron and the semiconductor is termed as n-type semiconductor. On the other hand if the majority charge carrier after doping is the hole, the semiconductor is termed as p-type semiconductor.

Solid state detectors are detectors or instruments used to detect nuclear and energetic particles such as alpha-particles, gamma radiation, etc. with higher energies. The threshold energy is determined by the thermal detector noise of the solid state detector. These detectors come in two main types namely solid state detector telescopes based on the energy loss in matter and the time of the flight telescope. These detectors are made up of semiconductor material, usually silicon [Wuest et al., 2007]. Also there are the foil and magnet types of particle detector systems based on the principles of solid state detectors.

Solid state detectors are made of semiconductors materials such as silicon by creating a p-n junction diode. A p-n junction diode is made up of an n-type semiconductor and a p-type semiconductor. The n-type and p-type semiconductors are made of the same material but different types of dopants and thus resulting in their names.

For an n-type the majority charge carriers are the electrons in the conduction band while holes in the valence band are the majority charge carriers in the p-type. The p-n junction diode has a region between the p-type and n-type semiconductors called the depletion region/layer. In this region electrons and holes from the n-type and the p-type respectively diffuses and recombines creating a neutral region (no charge carriers). There are neither free electrons nor holes in the conduction band and valence band respectively of the depletion region.

The depletion region (Fig. 3.1) behaves as the detector when the depletion region is large. In order to create a large depletion region, a reverse bias configuration is employed to the p-n junction. This can be achieved by connecting the p-n junction to an external voltage. The negative terminal of the power source is connected to the p-type while the positive terminal is connected to the n-type. This configuration gives us a minimal amount of current.

Due to the opposite polarities, the charge carriers are attracted to the opposite direction and thereby creating a larger depletion region needed for the purpose of detection. The reverse bias scenario employed is very vital due to its minimal amount of current flowing through the circuit and also necessary as the only current needed within the circuit should be one which is associated with the existence of an external ionizing particle. The creation of the larger depletion region in the set-up is important as it acts as our main detector.

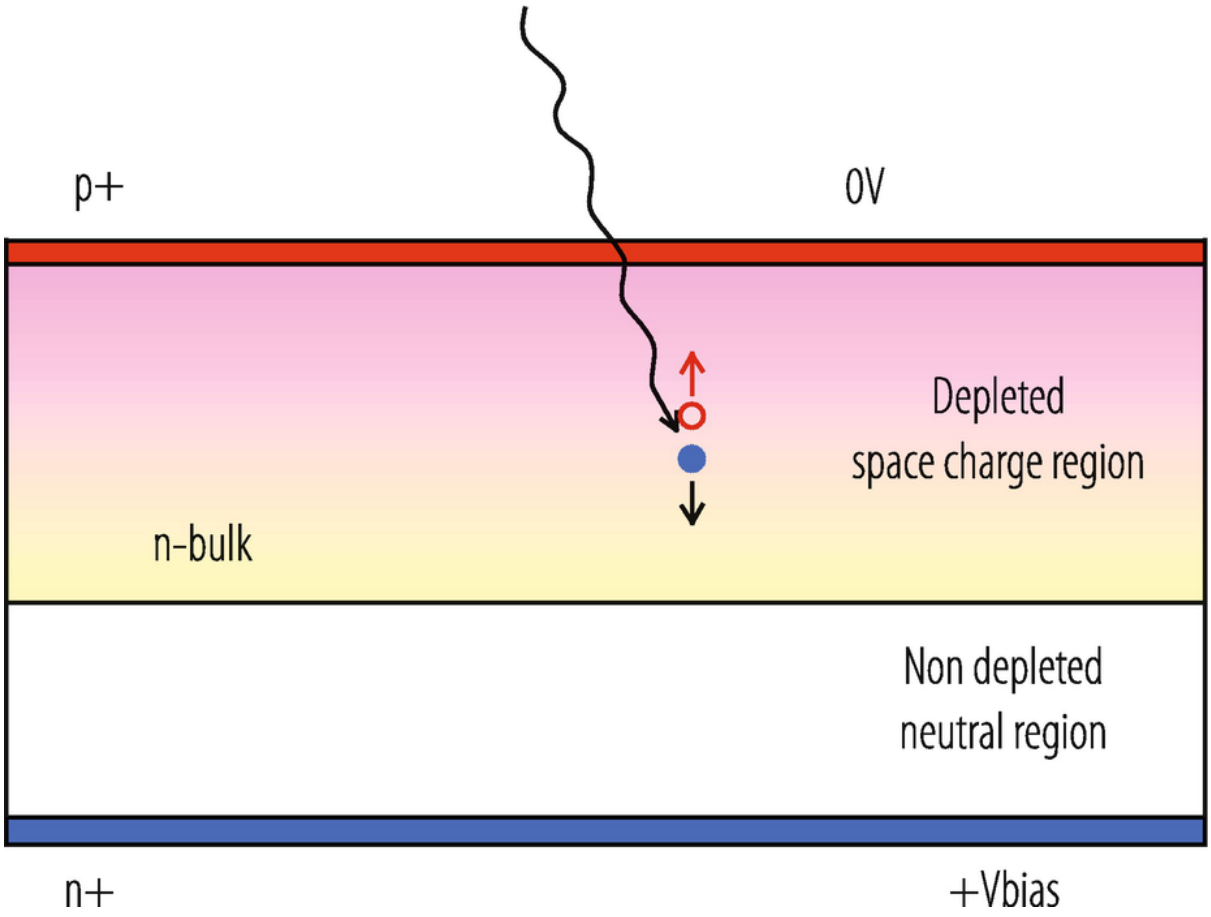

Fig. 3.1. A schematic diagram of a reverse biased p-n junction diode used as a particle detector. Image credit: Lutz and Klanner [2020]

3.1.1.2 How the semiconductor junction diode functions as a detector

Particles trapped within Earth's magnetic field, accelerated particles into space by means of solar flares and CMEs as well as galactic cosmic rays which are high energetic protons and heavy ions emanating outside our solar system are all space radiations. These radiations interact with semiconductor materials to create electron-hole pairs which are detectable as electric signals. Ionization occurs along the path of flight of an incident ray composed of charged particles by multiple collisions with electrons. The required average energy (3.6 eV for Si and 2.9 eV for Ge) needed to create an electron-hole pair is termed as ionization energy and this is weakly dependent on the type as well as the energy of the incident radiation. This excludes low-energy particles with energies comparable to the semiconductor band gap. The interpretation of these characteristics is such that the number of electron-hole pairs created with respect to the incident radiation energy is easily determined. This can only be achieved when the particle is fully stopped within the detector active volume [Rizzi et al., 2010].

The p-type and n-type semiconductors when brought into good thermodynamic contact create a p-n junction. The properties exhibited by this diode junction is very vital as it allows semiconductors to be used as electronic circuit materials as well as radiation measurements. These two extrinsic semiconductors (p-type and n-type) create a charge region known as the depleted charge region at their connecting point. This region comprises of two distinct zones. The two zones all have different charge carrier sites filled in them. One of the zones has filled electron acceptor sites not compensated by holes while the other zone has positively charged empty donor sites not compensated by electrons. In reducing the tendency for further charge diffusion, the depleted region therefore creates an electrical field [Rizzi et al., 2010].

The depleted region therefore acts like a high resistivity parallel plate ionization chamber, making it feasible to use the p-n junction (diode junction) for radiation detection. This is because the presence of an electric field causes the electron-hole pairs created inside the depleted region to traverse out of the region and their motion gives rise to an electrical signal. This makes the depleted region the sensitive volume of the semiconductor detector. In order to achieve all these, the p-n junction is connected in a reverse bias which makes the sensitive volume (depleted region) wider. Also a diode junction that is not biased can act like a detector but its performance is very poor. This is due to the fact that its sensitive volume thickness is small, has a very high junction capacitance and also has a very low electric field strength across the diode junction which is not enough to collect induced charge carriers which could potentially be lost due to trapping and recombination [Rizzi et al., 2010].

The solid state detector has the following advantages:

- Counts fast and operates at voltages dependent on the thickness of the detector and the resistivity of its material.
- Can be used in detecting very low energetic particles.
- Has a better energy resolution than detectors associated with very low current pulse.
- Is very small and compact.
- Has relatively low energy required (about 3 eV) for electron-hole pair generation.

Its disadvantages are as follows:

- Limitation to small thickness ~1 mm (for ion- implanted detectors)
- Susceptibility to damage by incident radiation.
- Detection energy threshold limited by the detector thermal noise.

Cooling the detector can significantly reduce the noise but this can significantly increase the size, mass and power of the instrument and also increase its complexity of design. [Wuest et al., 2007]

The limitation of detector thickness informs us that protons with high energies (> 14 MeV) will not stop in the detector. By arranging two or more silicon detectors as a stack we are able to measure energies of higher energy particles. The so-called Li-drifted junctions [e.g., Pell, 1960] can also be used to manufacture detectors with larger thicknesses. [Wuest et al., 2007]

3.1.2 Scintillators and their readout devices

The scintillation detector is a device consisting of mainly two parts namely scintillation material and a readout device, like a photodiode or a photomultiplier (see Fig. 3.2). It absorbs the energy of a charged particle upon entering and leads to the creation of light. This phenomenon is termed scintillation. Therefore, scintillation can be defined as the property of a material medium whereby the energy of a charged particle entering the medium is absorbed and leads to the emission of light. [Wuest et al., 2007, Flyck and Marmonier, 2002].

External particles collides with the molecules of the scintillation material upon entering. Energy transfer only happens after collisions between the external particle and the molecules of the scintillation material have taken place. Electrons in the valence band of the material absorb the energy and get excited to the conduction band with the aid of an applied voltage. There is always an emission of photon when the electron in the conduction band is de-excited back to the valence band. The material medium is therefore said to absorb energy of the incident particle and converts it to low energy photons. [Wuest et al., 2007, Flyck and Marmonier, 2002]

Different kinds of scintillation detectors use different kinds of scintillation media. For example a scintillator made of Caesium Iodide (CsI) is often used to detect protons and alpha particles.

The greater the energy of the incident radiation, the larger the number of photons created. The most efficient readout system for the scintillation light is the photomultiplier tube. Here, the photons are first focused into a photo cathode. The photocathode is made of material, which experiences photoelectric effect, i.e., the emission of electrons when electromagnetic radiation such as light hits the material. The photocathode material is placed on top of a photo-multiplier tube. The photons which are being focused on the photocathode results in photoelectric effect

and the emission of primary photoelectrons. The primary photoelectrons then enter the photo-multiplier tube with the main purpose to multiply the primary photoelectrons to a very high number. This results in a significant current pulse in the readout device connected to the system. [Wuest et al., 2007, Flyck and Marmonier, 2002]

3.1.2.1 Inorganic and Organic scintillators

There are two main types of scintillators namely inorganic and organic (e.g., plastic) scintillators. Inorganic scintillators consist of ionic crystals doped with activator atoms. Free electrons and holes as well as electron-ion pairs are produced as a result of having ionized particles traversing through the crystal of the system. These particles travel through the crystal until the encounter with activator atoms in their ground states and excite them to higher energies. There is an emission of scintillation photons as a result of having decay of activator back to the ground state. Inorganic scintillators are very useful and important due to their high stopping power for spectroscopy of high-energy particles. [Wuest et al., 2007]

Organic types of scintillators are used in more limited roles in spacecraft instruments. This system requires a greater amount of material to provide us with the same energy loss as we will get from a much smaller inorganic scintillator due to its lower density. A large detector will require extensive shielding which will result in obtaining a large and massive detector. One very useful area for plastic scintillators is as a veto counter/ active shield. A piece of plastic scintillator properly shaped is placed close to the sensors to be shielded. The signal that is obtained from the plastic scintillator behaves as a veto in a coincidence circuit with the detector signal. This is because a signal from the plastic indicates an out of aperture particle that must have struck the shielded sensors. Plastic scintillators are the best choice in the usage as a veto in coincidence circuits due to their short emission times. [Wuest et al., 2007]

Scintillators in general also have a relatively bad energy resolution relative to that of SSD's because

- much more energy is needed to generate a scintillation photon (40 – 50 eV) as compared to the energy needed to generate electron-hole pairs in silicon (3.6 eV).
- there are inefficiencies in transporting the photons to a light measuring device.
- light from scintillations is often measured by photodiode, which is not 100% effective.

These disadvantages are in addition to the device being relatively large and difficult in designing, packaging and shielding the sensor. [Wuest et al., 2007]

Figure 3.2 below illustrates a schematic diagram of a scintillation detector coupled to a photomultiplier tube. A high-energy incident particle (photon in this example) hits the scintillating crystal. This causes the release of low energy photons which are then converted into photoelectrons and multiplied in the photomultiplier. We will next explain the principle of a photomultiplier.

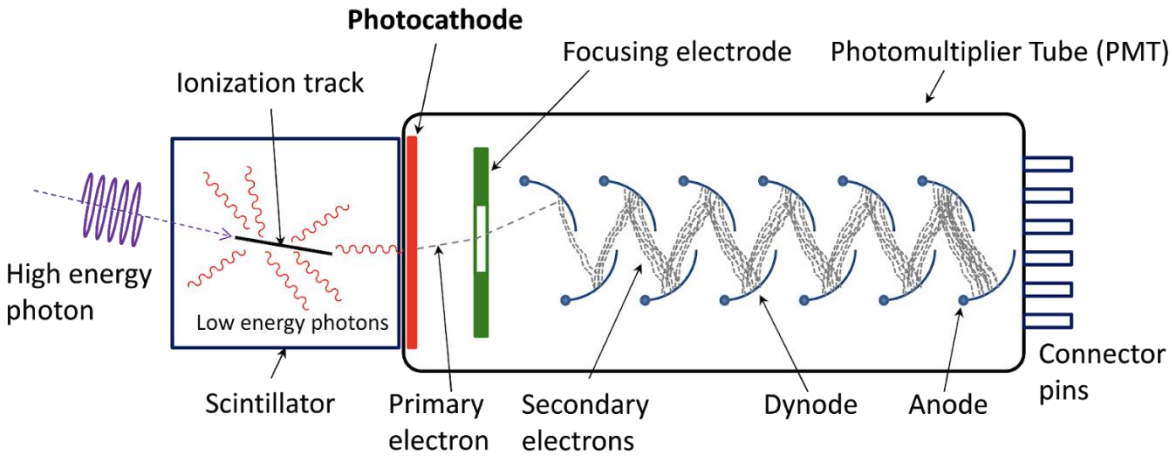

Fig.3.2. A schematic scintillation detector. Image credit By Qwerty123uiop, CC BY-SA 3.0, https://commons.wikimedia.org/w/index.php?curid=62426194

3.1.2.2 Principle or Mechanism of the photomultiplier tube

As the optical photons hit the photocathode, it leads to the emission of primary photoelectrons. These photoelectrons are also directed towards a particular electrode within the photo-multiplier tube via photoelectric effect. There are several electrodes also known as dynodes within the tube and all come with different voltages. As the primary photoelectrons hit the first dynode, it results in the emission of secondary photoelectrons which are also directed towards another dynode (second dynode). [Flyckt and Marmonier, 2002]

Since the first dynode and the second dynode have different potentials (voltage), there will be an electric field created which leads to the acceleration of the electrons towards the second dynode.

Any time the electrons strike a particular dynode they result in the emission of secondary photoelectrons. Again when these secondary photoelectrons reach the second dynode, the same

thing happens as in the first instance. With every single collision, a large number of secondary photoelectrons are emitted. The number of secondary photoelectrons at every stage increases exponentially. Therefore the main idea behind this construction is an exponential increase in the number of the photoelectrons.

Finally when the total number of electrons reaches the anode which is connected to the output signal, there is a large current pulse associated with it. The significant current pulse recorded is a result of the electrons being increased exponentially. The size of the current pulse detected by the electronic system connected to the detector is dependent on the number of incident primary photoelectrons created by the light photons. The primary electrons are also dependent on the number of optical photons generated in the scintillator material. Each photon creates one primary electron. The number of light photons is also dependent on the energy of the incident particle absorbed in the scintillator. Therefore by studying the detected current pulse, we can determine the energy of the incident particle that entered and was stopped in the scintillation material. [Flyck and Marmonier, 2002]

3.1.2.3 Photodiodes, avalanche photodiodes and silicon photomultipliers

Another vital instrument in the field of particle detection is the silicon photomultiplier (SiPM). This instrument exhibit properties of a semiconductor and it is regarded as a solid state photodetector. It has a configuration of over hundred integrated single-photon avalanche diodes (SPAD) termed as microcells or pixels. These integrated single-photon avalanche diode are arranged in an array [Gundacker and Heering, 2020]. SiPMs come in two distinct forms namely analog SiPM and digital SiPM. In analog SiPM, all the cells are independent and have a common readout in parallel configuration. Each cell in the analog SiPM has its own quenching resistor and is typically square shaped with approximately 10 micrometer [Acerbi et al., 2018] to 100 micrometer [Wagadarikar et al., 2013] in length. For the digital SiPM, each cell has its own readout electronics. [Gundacker and Heering, 2020].

The avalanche photodiode is the smallest microcell of the SiPM. It is a p-n junction diode and it is designed in a reverse bias above the breakdown voltage. There are three different regions of operation in this detector. The region of operation depends highly on the applied voltage across the diode.

To create an electron-hole pair, a striking photon is required. The electron-hole pair created by the effect of the impinging photon can be separated by an applied field. For a low voltage applied, where there is no further multiplication of the already generated electron-hole pairs, the diode is said to be operating in the photodiode regime.

When the applied reverse voltage is increased on the diode, the electric field becomes high and as such electrons gain enough energy and create secondary electron-hole pairs through impact ionization. In this stage, the diode is said to be operating in the avalanche photodiode regime. In this regime, only electrons are capable of generating secondary electron-hole pairs and the diode exhibits a gain from several tens to hundreds. The measured current in this regime is as well proportional to the number of detected photons or the generated electron-hole pairs. This is as a result for electrons being the only particle in this regime to have enough kinetic energy and create more electron-hole pairs. Just like the diode where current only flows in one direction, the avalanche also flows in one direction and it is self quenched (i.e., no external circuit needed to stop the avalanche).

For the third operating regime, a greater electric field than in the avalanche photodiode regime is applied. The holes in this case are able to create secondary electron-hole pairs because they gain enough velocity due to the greater field applied. Holes will need a greater amount of electric field in order to create secondary particles because of their higher effective mass. This operating regime is employed in SiPMs. In this operating regime, the avalanche is not self quenched as it is in the avalanche photodiode regime. Therefore the avalanche is quenched by lowering the bias voltage below the breakdown voltage. The bias voltage has to be restored after quenching the avalanche in order to detect another photon.

3.1.3 Microchannel plates

The microchannel plate (MCP) is essentially a fast high gain amplifier for electrons with many parallel spatial channels for use in imaging application. It is sensitive not only to input electrons but also to other charged particles (i.e., ions/elementary particles) and electromagnetic radiation with short wavelength (high photon energy), i.e., from UV to soft X-rays. [Paschotta, 2021].

MCP is closely similar to an electron multiplier. This is because both devices exhibit similar work output by way of multiplying electrons through secondary emission with the aim of

intensifying a single particle (or photon). Additionally, MCP provides spatial resolution due to its many separate channels.

MCP is basically designed as a slab with a material property highly resistive (typically 2 mm thickness) and a regular array of tiny slots. These slots lead from one face to the opposite and are densely distributed over the entire MCP surface. Typical diameter of microchannels is approximately 10 micrometers, approximately 6 micrometer in high resolution MCP's. The microchannels are spaced apart by approximately 15 micrometers. The microchannels are designed to be parallel to each other and often enter the plate at an acute angle (8 degrees) from the normal to the surface.

The MCP by its nature functions as a particle amplifier. It is capable of multiplying a single striking particle into a cloud of electrons. An individual microchannel within the set-up becomes a continuous-dynode electron amplifier by applying a strong electric field across the MCP. A particle enters the channels via a tiny crevice and exits the channels on the opposite side of the plate where they are accrue on an anode. The collecting anode in most cases functions as the detector but the MCP also can be used in that regard (detector). Some types of the MCP are Chevron MCP consisting of two MCPs with angled channels and the Z-stack MCP consisting of three MCPs with channels aligned in a z-shape.
[https://en.wikipedia.org/wiki/Microchannel_plate_detector, accessed 11.7.2021]

3.2 Instrument Types

An energetic particle instrument may consist of different kinds of sensors designed with the idea to measure properties/characteristics of energetic particles such as their spectra, composition, time variations and directional distributions over a broad range of energies. In this section, the Solar Orbiter/Energetic Particle Detector (EPD) is reviewed as a comprehensive example of an instrument suite measuring energies from suprathermal to relativistic range.

The Solar Orbiter/EPD employs several different techniques in energetic particle detection. It consists of a number of units namely

- Supra-Thermal Electrons and Protons (STEP)
- Supra-thermal Ion Spectrograph (SIS)
- Electron Proton Telescope (EPT)

- High Energy Telescope (HET)

In addition to these sensor units, the suite has a common Instrument Control Unit (ICU). The properties of the sensor units are listed in Table 3.1. It lists the geometric factor (GF), the number of apertures, the Field of View (FOV) size, the energy range and maximum time resolution of the sensor unit. The GF (measured in cm^2 sr) of the sensor unit is determined by the solid angle covered by the FOV and also the areas of the active detectors. It is the conversion factor applied to get from counting rate (measured in s^{-1}) to particle flux (measured in cm^{-2} sr^{-1} s^{-1}).

Table 3.1. Properties of the EPD instrument.

Property	**STEP**	**SIS**	**EPT**	**HET**
Geom. factor (cm² sr)	8.10^{-3}	0.2	0.01	0.27
Number of apertures	1	2	2x2	2x2
FOV(size/aperture)	28ºx54º	22º	30º	43º
Energy range	e-: 2-160 keV Ions: 4-160 keV	14 keV/n - 20 MeV/n	e-: 25-400 keV H:0.025-6 MeV He4: 1.5-6MeVn	e-: 0.3-30 MeV H, He4: 7-100 MeV/n CNO: 13-240 MeV/n
Max. time resolution (s)	1	3	1	1

3.2.1 Broom magnet method (EPD/EPT and EPD/STEP)

The purpose of the STEP sensor is to measure protons and electrons at suprathermal energies. Suprathermal energy can simply be defined as an energy greater than that associated with a thermal population of the same species. STEP measures the lowest energies in the EPD suite.

Principles and technologies used by other space-borne instruments in the past are employed for this purpose. The basic detection principle of the STEP sensor is quite similar to a number of other sensors on different instruments such as the LION/COSTEP sensor on the solar

heliospheric observatory (SOHO), the SEPT sensor on the Solar Terrestrial Relations Laboratory (STEREO) or EPT sensor of the EPD suite itself.

The STEP sensor engages two co-aligned sensor heads with parallel fields of view. Of the two co-aligned sensor heads, one contains a permanent magnet with the aim of deflecting electrons out of the nominal field of view and only measures particles in the nominal energy range other than electrons (i.e., ions). This sensor head is termed as the Magnet Channel (MC).

While the magnet channel does not measure electrons, the second sensor head known as the Integral channel (IC) measures electrons in addition to ions. The difference in the signals of the measurement of these two sensor heads provides us with the electron flux in the supra-thermal energy range [Rodriguez-Pacheco et al., 2020].

Detection principle

In order to be able to measure a particle's kinetic energy, the two sensor heads each have a solid state detector (SSD) with an ultra-thin window and several pixels based on technology used for STE instrument on STEREO. This configuration allows particle energy determination in the suprathermal energy range (3 keV – 65 keV). A small pinhole is utilized inside the sensor heads in order to achieve an angular resolution of the particles hitting the different pixels of the sensor.

The two sensor heads (MC and IC) are together mounted on a common electronics box and the electronics box is also mounted on the -y-deck of the spacecraft. The reason the sensor heads are mounted is for both fields of view to point into the direction of the average nominal Parker spiral and as such the bore-sight directions are tilted by an angle of 35º in the spacecraft's x-y plane towards the y-axis.

For the magnet method, a permanent magnet is placed above one of the two detectors. The magnet generates magnetic fields across the detectors. For this method, ions are able to travel through the magnetic fields and get detected by the detectors without much deflection. On the other hand, this method affects electrons which are not able to go through the magnetic fields but rather they are deflected and never get to the detectors. Electrons are affected by the magnetic field because of their low mass. Thus, we are able to say a particle is an ion when it is detected by the STEP magnetic channel [Rodriguez-Pacheco et al., 2020].

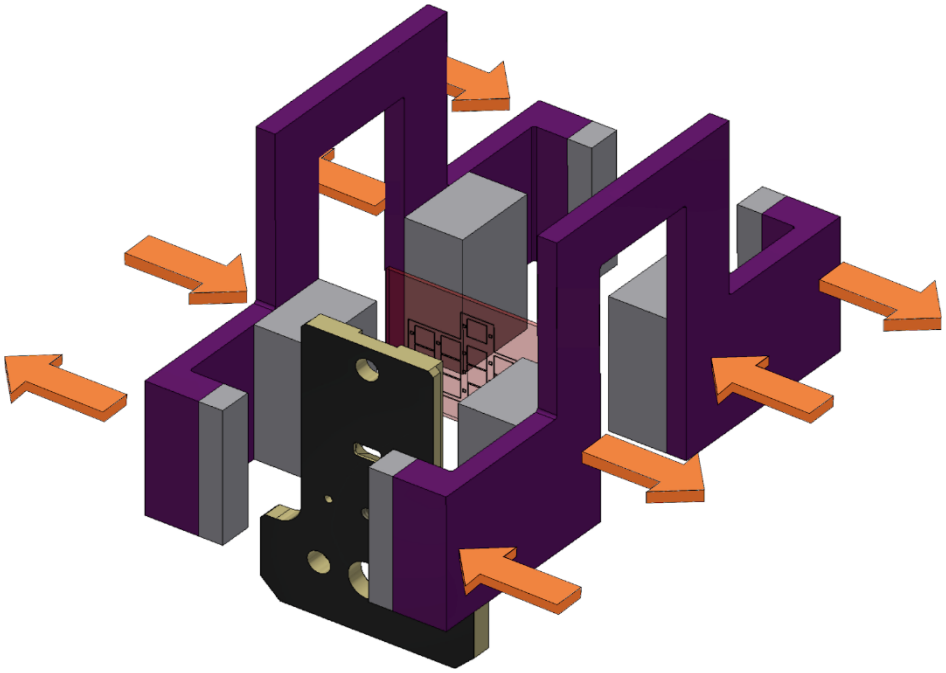

Fig. 3.3. CAD overview of the STEP magnet channel. Image credit: Rodriguez-Pacheco et al. [2020] http://espada.uah.es/epd/STEP.php

The structure of the STEP magnet channel is depicted in Fig. 3.3. The black and beige coloured structure is the pinhole. The purple coloured structure illustrates the magnet yokes while the gray structures represent the magnets in the sensor head. Each magnetic field line has an orientation illustrated by the orange arrows. The integral channel misses the magnets as well their yokes. [Rodiguez-Pacheco et al., 2020]

3.2.2 Below foil detection method (EPD/ EPT)

Just like the STEP, the EPT has a magnet channel but instead of an integral channel it has its other sensor covered with a foil. This technique is a characteristic of the STEREO/SEPT. This technique also helps to distinguish electrons and protons as in the case of STEP. It detects electrons within the energy range from 20 keV to 400 keV and protons in the energy range from 60 keV to 7000 keV. Basically this instrument is designed to cover up the gap between low energy particles measured by STEP and high energy particles measured by HET.

In this configuration, closely spaced detectors having two telescopes with two layers pointing in the same direction are used. The foil is usually very thin while the detectors are thick. In the case of a foil, electrons with energy E< 400 keV will simply go through the foil and get to the detector while protons at E < 400 keV will be stopped by the foil. The energy detected for electrons stopping in the first detector layer will be less than 400 keV, whereas protons are stopped in the first detector layer at higher energies (> 400 keV).

Operating principle

The EPT consists of two double-ended telescopes operating in an anticoincidence manner. It is also integrated with HET in one unit. The unit (EPT/HET) has a common housing and a readout electronics system. The unit provides directional information about an incoming particle. To achieve this information, the system is in two separate units (EPT/HET-1 and EPT/HET-2). The two units all have different directions to which they are pointed and also their locations on the spacecraft are different.

As mentioned earlier, the instrument employs the magnet/foil technique for particle separation. One of the SSDs is to look through the foil while the other looks through the magnetic deflection system. The foil is put in place to prevent low energy protons while it leaves electrons unaffected. The magnet is constructed purposely to detect ions and deflect electrons with low energy (< 400 keV). Low energy ions (20 keV to 7 MeV/n) will pass the magnetic field of the SSD and they finally stop in the detector below the magnetic field. Their fluxes are also measured. The ion energy contribution > 400 keV to the foil SSD can be computed and subtracted to obtain the electron fluxes. [Rodriguez-Pacheco et al., 2020]

Electrons with higher energy are able to traverse the magnetic field and get to the detector. But electrons with lower energies are affected by the field generated by the magnet (i.e., they are deflected). The trajectory of a high-energy electron is slightly bent and it is detected usually also on the second detector operated in anti-coincidence with the first one. In conclusion these two methods (foil and magnet) helps us measure the energy of particles and also separate the particles (electrons and protons). [Rodriguez-Pacheco et al., 2020].

3.2.3 Time-of-flight (TOF) method (EPD/SIS)

Time-of-flight is also another mechanism that is employed in the study of energetic particle detection. This mechanism measures the time a particle of known energy travels a given path length from a source to a detector to determine the particle's velocity and mass [Wuest et al., 2007].

The SIS is also an advanced instrument which has its principles based on the high resolution Ultra-Low Energy Isotope Spectrometer (ULEIS) instrument on the Advanced Composition Explorer (ACE). The SIS instrument is basically composed of two telescopes (SIS-A and SIS-B) which point in different directions. The two telescopes also share a common electronic readout system and it is mounted on the –y-deck of the spacecraft [Rodriguez-Pacheco et al., 2020].

Operating principle of SIS

In fig.3.4 below, the diagram illustrates a typical ion trajectory in the SIS instrument. The expected ion passes through three entrances namely: start-1, start-2 and stop foils. Secondary electrons are then emitted at each surface of the entrance. At the entrances, the secondary electrons are accelerated by an electric potential of 1 kV and also directed through isochronous paths onto microchannel plates (MCPs) providing fast start-1 start-2 and stop signals. The timing signals of the secondary electrons are used to estimate the ion time-of-flight (TOF) between foil combinations. There are three different time-of-flight measurements recorded by the system configuration namely: start-1 to stop (TOF-1), start-2 to stop (TOF-2) and start-1 to start-2 (TOF-3) [Rodriguez-Pacheco et al., 2020].

Theory

The energy for an ion measured by the solid state detector is given by

$$\mathrm{E} = \frac{1}{2}\,\mathrm{m}V^2 \qquad (1)$$

V and m are speed and mass of the particle respectively. The speed of the ion is measured by TOF section and given by

$$V = \frac{L}{\tau} \qquad (2)$$

L and τ are the path length and time of flight respectively. Then the mass of the ion can be determined by combining equations (1) and (2) to get:

$$m = 2E(\frac{\tau}{L})^2 \qquad (3)$$

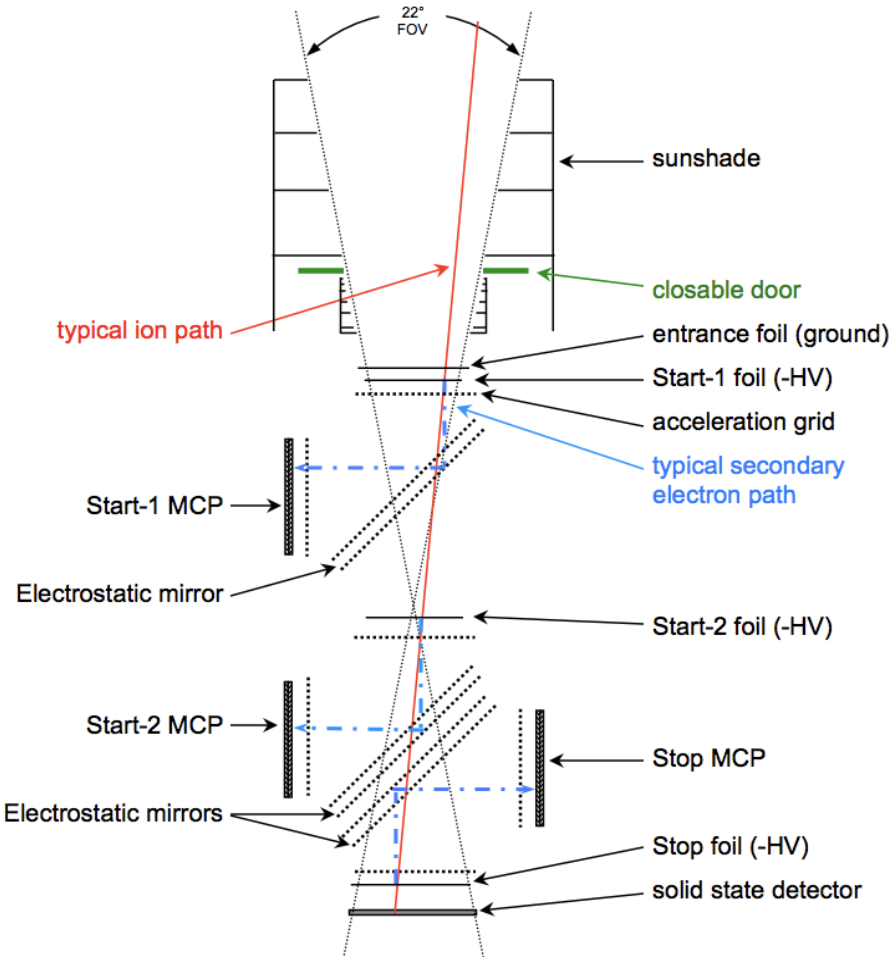

Fig.3.4. Cross-section over view of the SIS telescope. Image credit: http://espada.uah.es/epd/SIS.php

3.2.4 ∆E vs E method (multi-layer telescope) (EPD/HET)

Multi-layer telescopes are instruments designed to have layers of active detectors with different thickness forming a stack. The first active detector is usually the thinnest while the last is the thickest. The thickness of the detectors determines the minimum and maximum energy according to the range-energy relation in the detector material like silicon [Reames, 2017; Rodriguez-Pacheco et al., 2020].

As its name suggests, the High Energy Telescope (HET) is responsible for measuring particles (electrons, protons and heavy ions) located at the highest energy range of the EPD. The energy ranges from a few to hundreds of MeV/n and this comprises all energies of specific interest for studies in space weather. Aside measuring particles and their energies, the HET sensor also performs interesting measurements required in understanding the origin of high energy events at the Sun which is responsible for acceleration of particles to such high energies. These particles accelerated to such high energies are capable of penetrating the Earth's atmosphere leading to a GLE. Another interesting aspect of HET is its isotopic separation, which allows it to determine helium isotopes down to $^{3}He/^{4}He$ isotope ratio of about 1%.

The HET sensor has a configuration consisting of a double sided telescope head. It also shares the same electronics box system with the EPT sensor. On the spacecraft, there is the -y-deck and +y-deck where these EPD sensors are mounted. There are two separate EPT/HET units on the spacecraft. On the -y-deck, one of the units is mounted and pointed towards sun/anti-sunward along the average Parker spiral while on the +y-deck the second unit is mounted which is also set up to point out of the ecliptic making the HET sensor have a total of four viewing directions due to its design and configuration.

The HET sensor comprises four 300 μm thick silicon solid state detectors (SSDs) and also a high density scintillation crystal in its configuration. Its entrance collimator is protected by a Kapton foil and covered with a thick aluminium coating enabling it to reduce the low energy particle flux on its front detectors. As shown in Fig. 3.5, A1 and A2 are the front/back SSDs each having two segments. The middle SSDs are B1 and B2 with each also having three segments. The scintillation detector is labelled as C. The scintillation is a hexagonal BGO ($Bi_{14}\ Ge_3O_{12}$) crystal which is 2 cm thick and it is read out with two Hamamatsu S3590-09 photodiodes. To avoid loss of scintillation light, two Millipore and several layers of PTFE tape are used [Rodriguez-Pacheco et al., 2020].

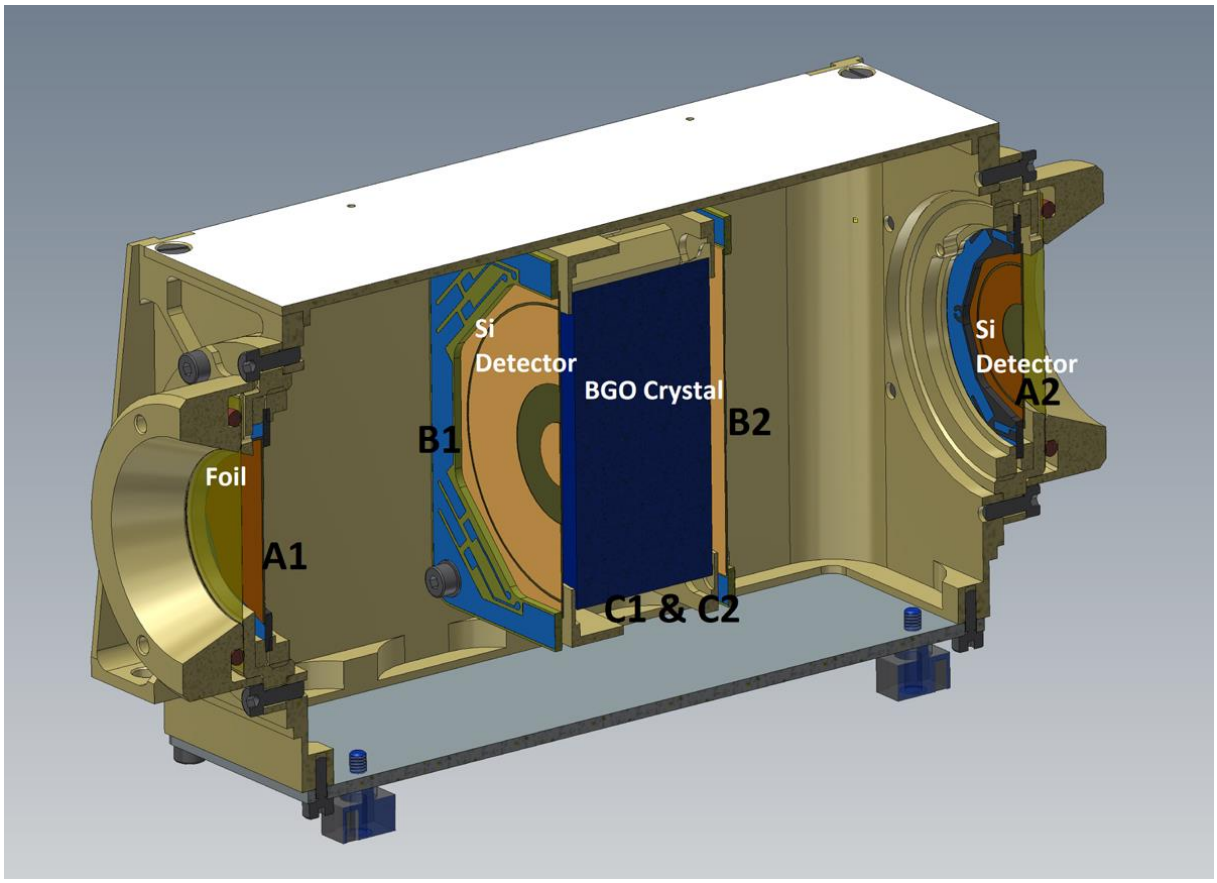

Fig. 3.5: cross-section of the HET sensor head. Image credit: Rodriguez-Pacheco et al., [2020].

ΔE vs E method

The Bethe- Bloch formula describes this method of particle detection. This formula describes the mean energy loss per distance travelled by a charged particle. These charged particles are protons, electrons and ions. The Bethe formula also describes the stopping power of the material these charged particles traverses. Electron energy loss is slightly different from the other charged particles because of their small mass. However electrons also suffer a lot much larger losses by Bremsstrahlung which requires the need for terms to be added to account for the loss.

Fast charged particles traversing through matter will interact with electrons of the atoms in the material. As a result of these interactions, the atoms are ionized which leads to an energy loss of the traversing charged particle. [https://en.wikipedia.org/wiki/Bethe_formula, accessed, 1.7.2021]

$$-\frac{dE}{dx} = \frac{4\pi}{m_e\, c^2} \cdot \frac{nz^2}{\beta^2} \cdot \left(\frac{e^2}{4\pi\varepsilon_o}\right)^2 \cdot \left[\ln\left(\frac{2m_e c^2\, \beta^2}{I.(1-\beta^2)}\right) - \beta^2\right] \qquad (4)$$

Equation 4 above represents the Bethe-Bloch equation which describes energy loss per distance travelled of charged particles as stated above. For particles with low energies (i.e., small velocities) $\beta = \frac{V}{c} << 1$ which will allow us to use $E = \frac{1}{2}mV^2$ to simplify equation (4). The logarithmic term from equation (4) changes only gradually in a limited energy range and can therefore be regarded as a constant, which eventually leads to equation (5) below.

Relevant Equations

$$-\frac{dE}{dx} = \frac{Z^2 m}{\mathrm{E}} C \qquad (5)$$

Equation (5) above is the approximate equation for the energy loss rate in a medium/material.
'Z' in the equation represents the nuclear charge of the particle (for hydrogen its 1 and 2 for helium).
'C' is a constant that depends on the medium/material.
'E' is the energy.
'm' is the mass

$$\Delta E_1 = \left(-\frac{dE}{dx}\right)\Delta x = C\Delta x \frac{Z^2 m}{\mathrm{E}} \qquad (6)$$

Equation (6) is used to determine particle energy losses in each layer of the detector.
'Δx' represents the thickness of the layers. If the thickness Δx of the front element is small compared to the range of the incident particle, then the energy loss ΔE is approximately equal to (-dE/dx) Δx. Combining the constant and the layer thickness gives the energy loss of an ion in the detector layer as a function of particle energy in the layer as:

$$\Delta E_1(\mathrm{E}) = D \frac{Z^2 m}{\mathrm{E}} \qquad (7)$$

We can see that for all species of different charge (z) and mass (m) the energy loss as a function of energy follows a hyperbolic curve and these curves are separated by the coefficient$z^2 m$. This is also clearly visible in Fig. 3.6.

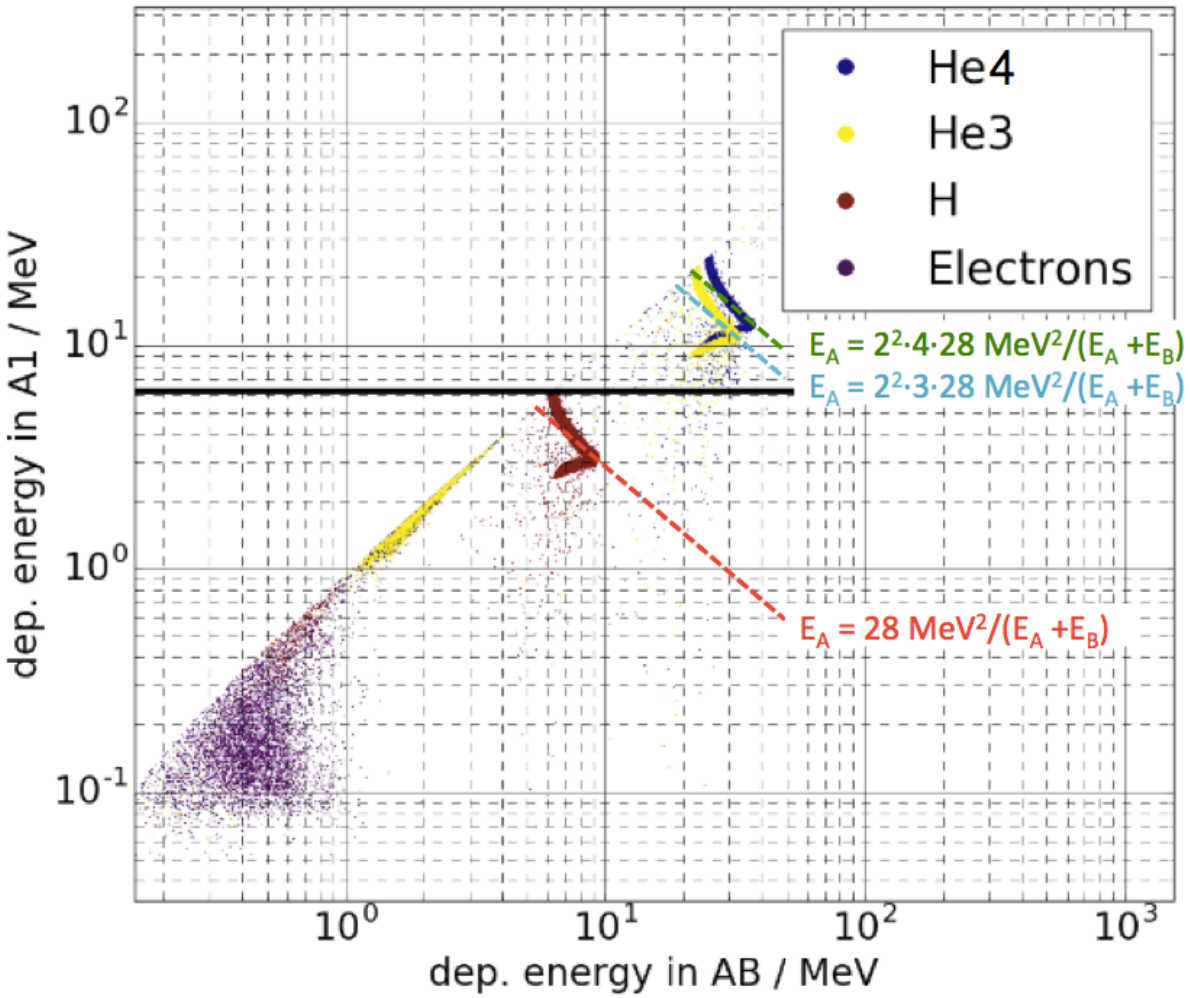

Fig. 3.6 A plot for the high particle flux. The black line illustrates the high particle flux cut for the HET ABnC trigger. Image credit: Adapted from Rodriguez-Pacheco et al. [2020] by R. Vainio

Figure3.6 above is a plot of simulation results illustrating the ΔE v E method technique of particle detection in HET. This detection mechanism/principle is very useful as it also a means of particle separation (i.e., protons, electrons and ions). The approximate proton track is $\frac{28\ MeV^2}{E}$. The ion species (3He and 4He) tracks are obtained by multiplying the proton track curve by a factor of $Z^2 m$ of these species.

4. A Design of a Particle Telescope

In the field of space physics, satellite instruments are the main tool for obtaining observational results on energetic particles. These instruments come in different forms and types depending on their specific target or goal. Examples of the targeted goal. In building these instruments, a lot of factors (intrinsic and extrinsic) are taken into account in order to meet the targeted goal. One very vital thing which is also taken into account is the kind of detector material used in the design. Recent instruments are designed and built using semiconductor materials due to their excellent properties and characteristics. As reviewed above, scintillators are used as well.

The typical choice of semiconductor material used in energetic particle detection is silicon. Germanium requires cooling in order to operate as a proper semiconductor and for that reason it is used for gamma-rays only for its superior stopping power relative to silicon. Silicon needs a maximum of 3.6 eV energy to create electron-hole pair which makes it the ultimate choice of semiconductor material. One other reason why semiconductor materials are now used in designing space instruments is the fact that information can be kept or stored for a long period of time without losing their performance.

In this chapter, I will optimise the design of a particle telescope similar to the RADMON instrument on Aalto-1 student satellite (Kestilä et al. 2013). The RADMON instrument consist of a stack of one Si-detector and a CsI(TI) scintillator with photodiode readout. The stack is under an aluminium window preventing low-energy particles and photons from entering the detector. The present telescope will have five layers for which the particle will penetrate. The first layer is the kapton polyimide film (foil) while the remaining four layers are made of Si-detectors and a CsI(TI) detector. The Caesium iodide detector is the last detector in the design and has a much greater thickness than all the layers. The thickness of the layers increases with depth (going downwards the telescope). With this configuration, we are able to determine the energies at which the incident particle (proton) penetrates each layer (detector) of the telescope. Furthermore the thicknesses of the design were carefully selected in order to achieve a desired energy resolution at each detector layer of the telescope. The fifth detector in the stack is made of Si and operated in an anti-coincidence technique in order to identify all particles traversing through the detectors in the telescope. Such particles would otherwise have their energies and species not well identified.

4.1 Methodology

In this section, my task was to optimise a design of a particle telescope having a foil, three Si detectors and CsI scintillator detector. The design also has readout photodiodes positioned at the sides which allows particles penetrating the CsI detector have a direct hit at the anti-coincidence (AC) placed below the stack, as shown in Fig. 4.1.

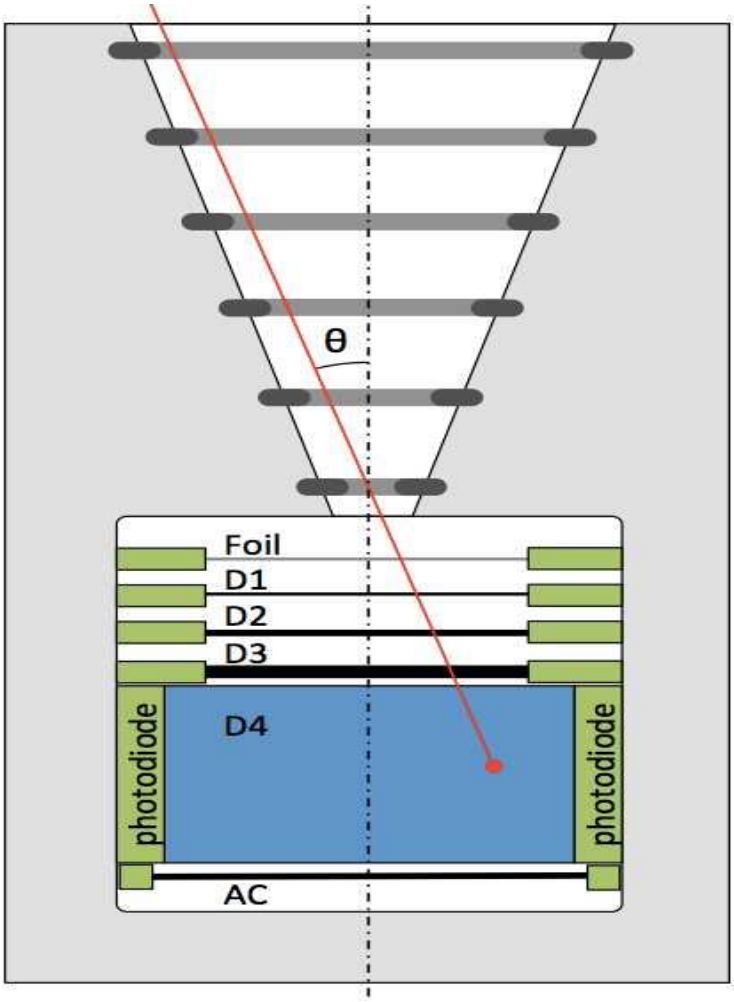

Fig.4.1 : Schematic RADMON-2 design also including the collimator structure limiting the angles of incidence. Image credit: Rami Vainio.

In this telescope design, my task was to first of all optimise the instrument based on a stack of three Si detectors (D1 – D3) and a CsI scintillator (D4). This optimisation of the instrument was necessary because my aim was to have the particle telescope measure protons at >5 MeV energies and also have a resolution of about 40% (0.4) in particle energies stopping within the three Si detector layers. The thickness of CsI scintillator used in the design was 1 cm and this

CsI scintillator is the bottom-most layer of the entire stack (like in RADMON). The foil thickness of the particle telescope was also determined as well as the optimal thicknesses of the three Si detector layers using a combination of 200 μm and 350 μm layers of silicon which correspond to detector thicknesses that are readily available in Space Research Laboratory.

Since I wanted to have the proton detection threshold energy in D1 at approximately 5 MeV, I therefore used the PSTAR tool [https://physics.nist.gov/PhysRefData/Star/Text/PSTAR.html], which provides the proton range as a function of energy in various media, to determine the optimal Kapton foil thickness. This was achieved by selecting the material Kapton foil within the PSTAR tool as well as the threshold energy (5 MeV). The tool shows a plot and a table listing the energies with their corresponding ranges in units of g/cm^2. For this design, I had the range for the Kapton foil to be $5.04 \times 10^{-2}\ g/cm^2$ which corresponded to the energy 5 MeV. This range of the foil material was then converted to its equivalence in Si using the expression below;

$$\frac{5.04 \times 10^{-2}\ g/cm^2}{2.33\ g/cm^3} = 0.0216\ cm$$

where $2.33\ g/cm^3$ is the Silicon density.

The pre-determined thickness used for CsI was 1 cm. This thickness is equal to 4.51 g/cm^2 in CsI (density 4.51 g/cm^3). This range of 4.51 g/cm^2 corresponded to an energy of 51.21 MeV from the PSTAR tool using CsI as the medium. The energy (51.21 MeV) corresponding to the thickness in CsI medium was then fed again into the PSTAR tool but this time using silicon as the medium. From the proton range table, the range in g/cm^2 corresponding to the energy of 51.21 MeV was 2.965 g/cm^2. This thickness was also converted to its Si-equivalent thickness in cm using the expression below;

$$\frac{2.965\ g/cm^2}{2.33\ g/cm^3} = 1.273\ cm$$

These conversions were necessary in order to be able to use a single energy-range relation during the optimisation exercise (i.e., that of proton in silicon).

The next step of the exercise was to choose combination of values as stated earlier for the Si detector thicknesses (D1 – D3) and calculate the energies of protons that are able to penetrate each of the layers of the three Si detectors. This optimisation was done having in mind the

desired energy resolution of 40% to be achieved at each of the Si detector layers. Several combinations were done before finally the most optimal thicknesses were settled on.

The energies of the protons penetrating at each detector layer was calculated using the range-energy relation, E(R), which I obtained from my supervisor (Prof. Rami Vainio). The range-energy relation, E(R), is given by

$$E(R) = \left(\sqrt{\frac{R}{k} + E_O^{2\alpha}} - E_O^{\alpha}\right)^{\frac{1}{\alpha}}$$

E is the measured energy loss for the penetrating particle at each detector layer.
R is the range (obtained from the traversed detector thicknesses at each layer)
K is a constant with value of 0.00258 $gcm^{-2}\ MeV^{-2\alpha}$
α is a constant with value of 0.839
E_o is a constant with value of 0.191 MeV.
This relation is a mathematical fit to the results of PSTAR for protons in silicon.

Incident proton energies for two different angles (see Fig. 4.1) were calculated (i.e., $\theta = 0°\ and\ 25°$). The energies were first calculated for protons incident on the detectors normally (i.e., $\theta = 0°$). For a proton stopping in D1, its range is between the foil thickness and the sum of the foil thickness and D1 thickness. For protons stopping in D2, the range is between the sum of the thicknesses of the foil and D1 and the sum of the thicknesses of ths foil, D1 and D2. For protons stopping in D3 and D4 the ranges are between the summed thicknesses of foil + D1 + D3 and foil +D1 +D2 +D3; and foil + D1 + D2 + D3 and foil + D1 + D2 + D3 + D4; respectively.

E1 and E2 are energies that were calculated using the E(R) relation. They are defined as energies of protons just reaching a detector layer and just penetrating it respectively. The width of the energy channels of protons stopping in D1, D2 and D3 were also calculated using the relation $\Delta E = E2 - E1$. This calculation was done for each stopping condition. The effective energies, E_{eff} of the channels were also calculated as a geometric mean of the boundaries using the relation;

$$E_{eff} = \sqrt{E1 \times E2}$$

Finally I used the results obtained from ΔE and E_{eff} to calculate the energy resolution for each detector layer and compared them to 40% (0.4). The energy resolution was calculated using the relation $\frac{\Delta E}{E_{eff}}$.

The energy calculation exercise was then repeated for particles with zenith angle of 25°. This is regarded as maximally inclined proton trajectory passing through the collimator to the detector stack. The corresponding ranges for this condition is obtained from the quotient of the values of 0° and cos 25° (i.e., $\frac{R(0°)}{\cos 25°}$). Finally, the final energies E1 and E2 were calculated as the mean of the values obtained with $0° \; and \; 25°$. Also ΔE and E_{eff} were also obtained from the mean values of the 0° and 25° conditions.

4.2 Results

Table 4.1 gives a summary on the telescope design with the various layer thickness and energies. The choice of the respective detector thickness was due to the fact that I want to have an energy resolution of about 0.4 at D1, D2 and D3. Several different combinations of detector layer thicknesses were tried until the optimal thicknesses, as combinations of 200 μm and 350 μm thick detectors were found. Note that the resulting optimal D3 detector would be a combination of two 350 μm detectors.

From table 4.1 again, it would be seen that, for a particle (proton) to penetrate the foil material with thickness of 0.0216 cm, the particle will need an energy of 4.9733 MeV. That is the energy which is detected or recorded at D1. For an incident particle to go through the entire silicon detector stack, it needs an energy of 15.0600 MeV which is the energy needed for the proton to reach D4 (CsI). This scenario is for an incident particle (proton) which traverses through the telescope perpendicular to the detectors.

Table 4.1. Detector thicknesses and energies. (θ= 0º)

	d [cm (Si)]	R [cm (Si)]	R [gcm^{-2}(Si)]	E1 [MeV]	E2 [MeV]	Eeff [MeV]	ΔE/Eeff
Foil	0.0216	0.0216	0.05041		4.9733		
D1 (Si)	0.0200	0.0416	0.09690	4.9733	7.2950	6.023	0.386
D2 (Si)	0.0350	0.0766	0.17850	7.2950	10.3810	8.702	0.355
D3 (Si)	0.0700	0.1466	0.34160	10.3810	15.0600	12.504	0.374
D4 (CsI)	1.2730	1.4196	3.30800	15.0600	54.5040	28.650	1.377

Tables 4.2 and 4.3 represent ranges and energies for incident particles hitting the detectors at an angle 25º and average energies per stopping detector respectively. Particles (protons) traversing through the detectors at an angle will need slightly greater energy to be detected as compared to particles traversing perpendicular to the detectors. The higher the angle of incidence the higher the ranges and energies required for the particle to traverse through the detectors. Table 4.4 represents channel boundary energies for the various detector layers. These channel boundary energies are the minimum and maximum required energies a particle must have in order to be able to be detected in the respective detector layers, if the angle of incidence is between $0° \; and \; 25°$. Note that the design includes a collimator structure which limits the angles of incidence of the particles (see Fig. 4.1)

Table 4.2. Detector thickness and energies (θ =25º)

	d [cm (Si)]	R [cm(Si)]	R [g/cm²(Si)]	E1 [MeV]	E2 [MeV]	E eff [MeV]	ΔE/E eff
foil	0.0216	0.0238	0.05545		5..2654		
D1	0.0200	0.0459	0.10695	5.2654	7.7238	6.3772	0.3855
D2	0.0350	0.0845	0.19689	7.7238	10.9826	9.2102	0.3538

D3	0.0700	0.1618	0.37699	10.9826	15.9312	13.2275	0.3741
D4(CsI)	1.2730	1.5664	3.64971	15.9312	57.6101	30.2952	1.3758

Table 4.3. Average energies per stopping detector in the various detector layers.

Average energies per stopping detector	E1 [MeV]	E2 [MeV]	Eeff [MeV]	ΔE/Eeff
D1	5.12	7.51	6.20	0.39
D2	7.51	10.68	8.96	0.35
D3	10.68	15.50	12.87	0.37
D4	15.50	56.07	29.48	1.38

Table 4.4. Channel boundary energies for the various layers.

Detector	E1(0º) [MeV]	E1(25º) [MeV}	E2(0º) [MeV]	E2(25º) [MeV]	Channel boundary energy, E1	Channel boundary energy, E2
D1	4.9733	5.2654	7.9250	7.7238	5.1194	7.8244
D2	7.2950	7.7238	10.3810	10.9826	7.5094	10.6818
D3	10.3810	10.9826	15.0600	15.9312	10.6818	15.4956
D4	15.0600	15.9312	54.5040	57.4956	15.4956	56.0571

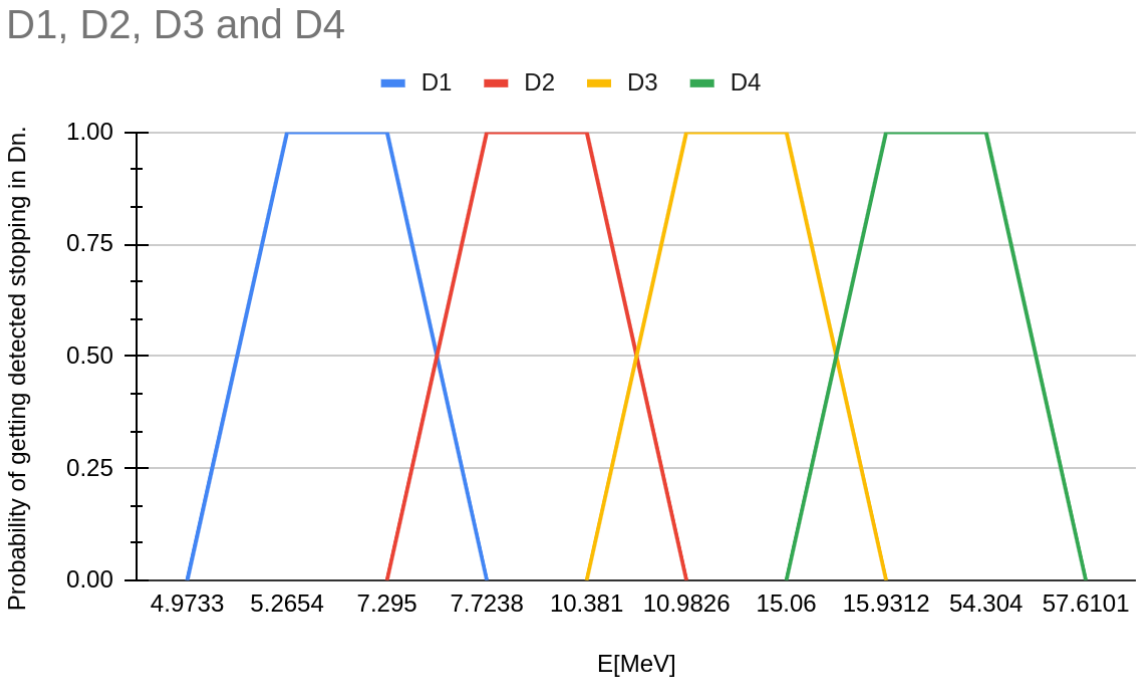

Fig.4.2. A graph showing the probability of protons being stopped in D1, D2, D3 and D4 as a function of energy.

Figure 4.2 above is the graph showing the probability of a proton being stopped at every point in time in the detector layers at certain range of energies which the particle should possess. From the graph, it can be seen that, for a proton to be always stopped in the first detector (D1) the proton must have an energy range of 5.2654 MeV and 7.2950 MeV (i.e., E1(25°) and E2(0°). All energies between that ranges for a proton can also be stopped in the first detector (D1). A proton with energy below 4.9733 MeV has a probability of zero of being detected which means such a proton cannot be stopped in the first detector. Protons with energies from 7.7238 MeV to 10.3810 MeV are those which are always stopped in the second detector (D2) because they have the required energy for a proton to penetrate through detector one (D1) and be stopped in detector two (D2). From the graph, we can see that there is also an energy range between 7.295 and 7.7238 MeV where the proton can be stopping in either one of the detectors, depending on its angle of incidence. This pattern can also be seen in the remaining detectors (D3 and D4) as well.

5. Summary and Conclusion

Energetic charged particles in space are not only from our Sun but these particles have other sources such as interplanetary space, the supernova explosions in Milky Way, etc., as reviewed in chapter 2. Solar energetic particles occur in events that are classified under two distinct categories, namely gradual events and impulsive events. While the gradual events occur over a long period of time (days), the impulsive events occur over a short period of time (hours). Also the gradual events are proton rich while the impulsive events are electron rich. SEPs were first thought to emanate only from solar flares until it was also determined that CMEs also produce SEPs.

Semiconductor materials have become the most suitable materials used these days in designing and the construction of particle detectors. These detectors are termed solid state detectors and the most common ones used are silicon (Si) and germanium (Ge). But the most used in our field of work (energetic particle detection) is the silicon. Germanium on the other hand to act as proper semiconductor will need cooling and as such used for gamma-rays only. Semiconductor materials are doped with materials which makes them have positive charge (holes) as majority charge carriers on one side and the other side doped with material making them have negative charge (electrons) as majority charge carriers. The majority positive side is termed the p-type and the majority negative side is the n-type. The doped materials brought together now become what we call the p-n junction diode and it is connected in a reverse bias mode to act as a detector. Depending on the kind of particle to be detected, detectors are designed to detect employing different techniques such as below foil detection method, broom magnet method, multiple layer detection method, etc.. For the foil/magnet method detection technique ions are stopped by the foil and electrons penetrate the foil. But when there is the magnet in place, electrons are deflected by the magnetic field due to their low mass. This technique (foil/magnet method) measures the energy of the particle and as well differentiate between the particles (electrons and protons).

The particle telescope design optimisation carried out in this work was successful as it provided with the desired energy resolution and energy range. This was possible with the thicknesses of the silicon detectors I selected to work with. In order to better understand the implications of the particle telescope design, future researchers and studies could also look to address the relationship between ranges at angles greater than 25º and their associated energies, effective

energies, energy channel width and their energy resolution. Other particle species such as electrons and alpha particles should be considered as well.

6. References

Acerbi et al., (2018): High efficiency, ultra-high density silicon photomultipliers. IEEE J. Sel. Top. Quantum electron. 24 3800608

Aurass, H. et al., (2002): Shock excited radio burst from reconnection outflow jet. Astron. Astrophys. 384, 273-281. Doi: 10.1051/0004-6361: 20011735.

Bertuccio, G., (2005): Prospect for energy resolving x-ray imaging with compound semiconductor pixel detectors. Nucl. Instrum. Meth. Phys. Res., 546:232-241

Blake, J.B. et al., (1992): Geophys. Res. Letters 19, 821.

Buzhan et al., (2003): Silicon photomultiplier and its possible applications. Nucl. Instrum. Methods Phys. Res. A 504 48-52.

Desai, M. Giacalone, J.(2016); Large gradual solar energetic particle events. Living Rev. Sol. Phys. 13:3, doi: 10.1007/s41116-016-0002-5.

Flyck, S. O. and Marmonier, C. (2002): Photomultiplier tube principles and applications. Philips Photonics, Brive, France.

Forbes, T.G. (1986): Fast shock formation in line-tied magnetic reconnection models of solar flares. Astrophys. J. 305, 559-563. Doi: 10.1086/164268.

Forbush S.E. (1964): Three unusual cosmic rays increase possibly due to charged particles from the sun. Phys. Rev. 70:771-772. Doi: 10.1103/physRev.70:771

Frach et al., (2009): The digital silicon photomultiplier principle of operation and intrinsic detector performance. 2009 IEEE Nucl. Sci. Symp. Conf. Rec. (NSS/MIC) (Orlando, FL, 24 october – 1 November 2009) (Piscataway, NJ: IEEE) 1959 – 65.

Freden, S.C and White R.S, (1960): J. Geophys. Res. 65, 1377.

Gerrard, T.L and Stone E.C, (1993): New SEP-based solar abundances. Proc. 23rd internat. cosmic ray conf. (Calgary), 3, 384-387.

Golovin and Saveliev (2004): Novel type of avalanche photodetector with Geiger mode operation. Nucl. Instrum. Methods Phys. Res. A 518 560-4.

Gopalswamy, N. et al., (2002): APJ, 572, L 103

Gray et al., (2015): Observation and modelling of a termination shock in a solar eruption as a possible particle accelerator.

Herbert et al., (2006): First results of scintillator readout with silicon photomultiplier. IEEE Trans. Nucl. Sci. 53 389-94.

Hess, W.N, (1959): Phys. Rev. letters 3, 11.

https://spaceplace.nasa.gov/solar-activity/en/

Hu, S. (2017): Solar particle events and radiation exposure in space. In THREE Encyclopedia, NASA. http://three.jsc.nasa.gov/articles/Hu-SPEs.pdf

Hubert, F. et al., (1990): Range and stopping power tables for 2.5 – 500 MeV/nucleon heavy ions in solids. Atom. Dat. Nucl. Dat. Tables. 46, 1 (1990). Doi: 10.1016/0092-640x(90)90001-z

Hudson, M.K, et al., (1997): J. Geophys. Res. 102, 14 087

Hudson, M.K. et al., (1998): Adv. Space Res. 21(4), 597

Kahler et al., (1978): Prompt solar proton events and coronal mass ejections. Sol. Phys. 57:429-443. Doi: 10.1007/BF00160116

Kahler, S.W. (2001): J. Geophys. Res., 106, 20947

Kallenrode, M.B. (2003): Current views on impulsive and gradual solar energetic particle events. J. Phys. G. Nucl. Part Phys. 29:965—981, doi: 10.1088/0954-3899/29/5/316

Klecker, et al., (1984): Direct determination of ionic charge distribution of helium and iron in 3He rich solar energetic particle events. Astrophys. J., 281, 458-462.

Kunow, H., et al.(1991): Energetic particles in the inner solar system. In R. Schwenn and E. Marsch (eds): Physics of the inner Heliosphere 2. Springer: Berlin

Lee, M.A. et al., (2012): Space Sci. Rev., 173, 247

Leske, R.A et al., (2001): Mass fractionation in solar energetic particles and the isotopic composition of the corona.

Lingenfelter, R.E, (1963): J. Geophys. Res. 68, 5633.

Liu et al. (2016): In-depth study of single photon time resolution for the Philips digital silicon photomultiplier J. Instrum. 11 P06006.

Luhn, et al. (1987): The mean ionic charge of silicon in 3He rich solar flares. Astrophys. J., 317, 951-955.

Lutz G., Klanner R. (2020) Solid State Detectors. In F abjan C., Schopper H. (eds): Particle Physics Reference Library. Springer, Cham. https://doi.org/10.1007/978-3-030-35318-6_5

Mason, G.M. (2007): 3He-rich solar energetic particle events. Space sci. Rev. 130(1-4), 231-242.

Mewaldt, R.A and Stone E.C, (1989): Isotopic abundances of solar coronal material derived from solar energetic particle measurements. Astrophys. J. 337, 959-963.

Miller, J.A and A.F. Vinas, (1993): Ion acceleration and abundance enhancements by electron beam instabilities in impulsive solar flares. Astrophys. J., 412, 386-400.

Miller, J.A. et al., (1997): Critical issues for understanding particle acceleration in impulsive solar flares. J.Geophys. Res. 102, 14631-14660. Doi: 10.1029/97 JA00976.

Northrop, T.G., (1963): The adiabatic motion of charged particles. (New York:inter science)

Paschotta, R. (2021): Article on 'microchannel plates' in the RP Photonics Encyclopedia, 2021-03-31.

Pell, E.M. (1960): J. Applied phys. 31,291, doi: 10.1063/1.1735561.

Prettyman, T. H. (2014): in Encyclopedia of the Solar System (Third Edition)

Reames, D.V (1995), Solar energetic particles; a paradigm shift. Rev. Geophys. 33 (suppl): 585-589. Doi: 10.1029/95RG00188.

Reames, D.V (1999), Particle acceleration at the sun and in the heliosphere. Space sci. rev. 90:413-491. Doi: 10.1023/A:1005105831781

Reames, D.V (1999): Space Sci. Rev., 90, 413

Reames V.D, (2017): solar energetic particles.

Renker, D. and Lorenz, E. (2009): Advances in solid state photon detectors. J. Instrum. 4 P04004.

Renker, D. and Lorenz, E. (2020): Geiger mode avalanche photodiodes, history, properties and problems. Nucl. Instrum. Methods Phys. Res. A 567 48-56.

Rice, W.K.M. et al., (2003): Particle acceleration and coronal mass ejection driven shocks: shocks of arbitrary strength. J. Geophys. Res. 108(A10), SSH 5-1. doi: 10.1029/2002JA009756.

Rizzi, M. et al., (2010): J. Applied science, 10(23):3141-3155, semiconductor detectors and principles of radiation matter interaction.

Rizzi, M. et al., 2005: Novel microstrip system detectors for medical applications. WSEAS Trans. Biol. Biomed., 2:220-227

Rodrguez-Pacheco, J. et al., (2020): The energetic particle detector. Energetic particle instrument suite for the Solar Orbiter mission. Astron. Astrophys. 642,A7. https://doi.org/10.1051/0004-6361/201935287.

Singer, S.F, (1958): Phys. Rev. letters 1, 181.

Stefen, G. and Arjan, H., (2020): The silicon Photomultiplier: fundamental and applications of a modern solid state photo detector. Phys. Med. Biol. 65(2020) 17TR01

Wang, L. (2009): Solar impulsive energetic electron events (published dissertation). University of California, Berkeley.

Wagadarikar et al., (2013): Performance of low after pulsing probability multi pixel photon counters for time of flight positron emission tomography. IEEE Nucl. Sci. symp. and medical imaging conf. (2013 NSS/MIC) (Seoul, 27 October = 2 November 2013) (Piscataway, NJ: IEEE) pp1-5

Williams, D.L et al., (1998): Solar energetic particle isotopic composition. Space sci. Rev., 85, 379-386.

Wuest, M., Evans, D.S. and Von Steiger, R. (eds). (2007): Calibration of particle instruments in space physics. Pp 32-76. SR-007. ISSI Scientific report.

Yougui, L. (2007): Practical Electron Microscopy and Database.

Zharkova, V.V. et al., (2011): Recent advances in understanding particle acceleration processes in solar flares. Space Sci. Rev. 159, 357-420. Doi: 10.1007/s11214.011.9803.y

https://physics.nist.gov/PhysRefData/Star/Text/PSTAR.html